This article has been accepted for publication in a future issue of this journal, but has not been fully edited. Content may change prior to final publication. Citation information: DOI 10.1109/TII.2020.2995742, IEEE Transactions on Industrial Informatics

Joint Planning of EV Fast Charging Stations and Power Distribution Systems with Balanced Traffic Flow Assignment

Wentao Yang, Weijia Liu, C. Y. Chung, *Fellow, IEEE*, and Fushuan Wen, *Senior Member, IEEE*

***Abstract* — To tackle the challenges introduced by the fast-growing charging demand of electric vehicles (EVs), the power distribution systems (PDSs) and fast charging stations (FCSs) of EVs should be planned and operated in a more coordinated fashion. However, existing planning approaches generally aim to minimize investment costs in PDSs while ignoring the risk of worsening traffic conditions. To overcome this research gap, this paper integrates the interests of traffic networks into PDS and FCS joint planning model to mitigate negative impacts on traffic conditions caused by installing FCSs. First, a novel microscopic method that is different from traditional assignment methods is proposed to simulate the influences of FCSs on traffic flows and EV charging loads. Then, a multi-objective joint planning model is developed to minimize both the planning costs and unbalanced traffic flows. A new bilayer Benders decomposition algorithm is designed to solve the proposed joint planning model. Numerical results on two practical systems in China validate the feasibility of our microscopic method by comparing the simulated results with real data. Compared with existing approaches, it is also demonstrated that the proposed joint planning approach helps to balance traffic flow assignments and relieve traffic congestion.**

***Index Terms* — electric vehicle (EV), bilayer expanded Benders decomposition, multi-agent-based microscopic traffic assignment model (MMTAM), joint planning, traffic flow assignment.**

NOMENCLATURE

Abbreviation

BPR	US Bureau of Public Roads
EV	Electric vehicle
FCS	Fast charging station
MMTAM	Multi-agent-based microscopic traffic assignment model
MINLP	Mixed-integer nonlinear programming
NSGA-II	Non-dominated sorting genetic algorithm II
PDS	Power distribution system
SOC	State of charge

Sets and Indexes

T/t	Set and index of operation time slot
$\Omega^{\mathrm{TN}}/i, j$	Set and indexes of traffic node
Ω^{TR}/ij	Set and index of traffic road
Ω^{AG}/k	Set and index of agent
Ω^{FCS}/q	Set and index of FCS
$\Omega^{\mathrm{B}}/u, v$	Set and indexes of buses in a PDS
Γ/τ	Set and index of planning stage
$\Omega^{\mathrm{FCS},\tau}$	Sets of candidate and existing FCSs
$\Omega^{\mathrm{PB},\tau}$, $\Omega^{\mathrm{EB},\tau}$	Sets of candidate and existing buses
$\Omega^{\mathrm{F},\tau}$, $\Omega^{\mathrm{S},\tau}$	Sets of feeder schemes and capacities schemes
$h^{(m)}$, m	Indexes of the inner and outer-layer iterations

Parameters and Variables

c^{τ}_{uv}, l^{τ}_{uv}, R^{τ}_{uv}	Feeder installation cost, length, and resistance
C^{AG}_{k}	Battery capacity of agent k
d^{A}	Duration days in a single planning stage
E^{AG}_{k}	Electricity consumption per km of agent k
$f^{\mathrm{RID}}_{k,t}$	Extra driving distance caused by charging
f^{FCS}, f^{UB}	Installation cost and the unbalance of traffic flow assignment
$f^{\mathrm{F},\tau}$, $f^{\Delta,\tau}$, $f^{\mathrm{B},\tau}$	Costs of installing feeders, electricity loss, and installing/reinforcing transformers
f^{PDS}	Total cost of planning PDS
$\boldsymbol{F}^{\tau}$	Matrix of traffic flows
L_{ij}, v^{0}_{ij}, c_{ij},	Length, maximum speed, and capacity of road
$F_{ij,t}$	Traffic flow of road ij
$n^{\mathrm{FAG}}_{q,t}$, $n^{\mathrm{SAG}}_{u,t}$,	Number of agents need fast and slow charging
$\underline{n}^{\mathrm{FCS},\tau}$	Minimum number of FCS installations
n^{FC}_{q} (n^{SC}_{u})	Number of fast (slow) charging devices
$O_{k,t}$, D_{q}	Locations of agent k and FCS q
$p_{ij,t}$	Index generated by the BPR function
P^{FC} (P^{SC})	Rated power of fast (slow) charging devices
$P^{\tau}_{u,t}$ ($Q^{\tau}_{u,t}$)	Net nodal active (reactive) power injection
$P^{\mathrm{L},\tau}_{u,t}$ ($Q^{\mathrm{L},\tau}_{u,t}$)	Nodal active (reactive) power load
$P^{\mathrm{S},\tau}_{u,t}$ ($Q^{\mathrm{S},\tau}_{u,t}$)	Nodal active (reactive) power generation
$P^{\mathrm{VS},\tau(m)}_{u,t}$, $P^{\mathrm{VL},\tau(m)}_{u,t}$	Nonnegative virtual power source and load during Benders iterations
$\boldsymbol{P}^{\mathrm{FCS},\tau}$, $\boldsymbol{P}^{\mathrm{CP},\tau}$	Matrixes of fast and slow charging load
R^{τ}_{u}, X^{τ}_{u}	Resistance and reactance of the feeder whose power receiving node is bus u
$S^{0,\tau}_{u}$	Initial capacity of bus u at stage τ
$S^{\tau}_{u,b}$	Capacity of installation scheme b
$S_{\text{th-1}}$, $S_{\text{th-2}}$	Two thresholds of SOC regarding battery safety
$t^{\mathrm{aver}}_{q,t}$	Waiting time of FCS q at time slot t
$\bar{t}_{k}$	Maximum desired waiting time of agent k
Δt	Length of time scale/slot
V_{B}	Rated voltage of a PDS
$V^{\tau}_{u,t}$ ($\underline{V}$, $\overline{V}$)	Voltage magnitude of bus u at time t and its limits
y^{τ}_{ua}	Feeder investment decision variable of scheme a
$z^{\mathrm{P},\tau}_{u,b}$ ($z^{\mathrm{E},\tau}_{u,b}$)	Installation/reinforcement decision variables of scheme b
α	The constant ratio of traffic flow to capacity

This work is jointly supported by the National Natural Science Foundation of China (No. U1910216), the National Key Research and Development Program of China (Basic Research Class) (No. 2017YFB0903000), the Natural Sciences and Engineering Research Council (NSERC) of Canada, and the Saskatchewan Power Corporation (SaskPower).

W. Yang is with the College of Electrical Engineering, Zhejiang University, Hangzhou 310027, China (e-mail: wentaoyang@zju.edu.cn).

W. Liu is with the Power System Engineering Center, National Renewable Energy Laboratory, Golden, CO 80401, USA (e-mail: liuweijiamarcel@gmail.com).

C. Y. Chung is with the Department of Electrical and Computer Engineering, University of Saskatchewan, Saskatoon S7N 5A9, Canada (e-mail: c.y.chung@usask.ca).

F. Wen is with the College of Electrical Engineering, Zhejiang University, Hangzhou 310027, China, and the Department of Electrical Power Engineering and Mechatronics, Tallinn University of Technology, Tallinn 19086, Estonia (e-mail: fu-shuan.wen@gmail.com).

This article has been accepted for publication in a future issue of this journal, but has not been fully edited. Content may change prior to final publication. Citation information: DOI 10.1109/TII.2020.2995742, IEEE Transactions on Industrial Informatics

γ	Fund discount rate
$\delta_q^{\mathrm{F},\tau}$, $\delta^{\mathrm{B},\tau}$	The land-use fee of FCS and substation
η^{AG}	Permeability of EVs/agents
$\lambda_{k,t}$, $S_{k,t}$	Charging status and SOC of agent k
$\mu^{\mathrm{F},\tau}$ ($\kappa^{\mathrm{F},\tau}$)	Installation (operating) cost of FCS
$\mu^{\mathrm{B},\tau}$ ($\kappa^{\mathrm{B},\tau}$)	Installation (operation) cost of substation
σ	Retail price of electricity
$\varphi_{q,u}^{\tau}$	Decision variable of selecting which bus to connecting FCS q
$\Re(\bullet)$	Unbalance function of traffic flow

I. Introduction

With ever-rising environmental concerns, such as the depletion of fossil energy, increasing carbon emissions, and rapidly growing energy demands [1], the replacement of fossil fuel vehicles has become a priority in the global energy transition. As an alternative transportation option, electric vehicles (EVs) are believed to reduce carbon emissions and support the vast integration of renewable energy. Many countries have already announced roadmap and policy support to replace traditional fossil fuel vehicles with EVs. For example, China's annual production capacity of EVs is expected to reach 2 million by 2020 [2], the German government has set a goal of having 1 million EVs by 2020, and the UK has announced its intention to completely phase out fossil fuel vehicles by 2040 [3].

At present, two technologies have been developed for EV charging, i.e., fast charging and slow charging [4]. Fast charging can significantly reduce charging time and extend the driving mileage of EVs. Hence, the planning and installation of fast-charging stations (FCSs) are vital to popularizing EVs. Several existing works, e.g., [5]-[7], have addressed the optimal siting and sizing of FCSs. However, they assumed the given power distribution system (PDS) has sufficient capacity to accommodate the increasing EV charging loads, which simplifies the investment of FCSs and should be considered impractical. Besides, due to the random charging behaviors of EVs, the charging demand at FCSs may be intermittent and thus challenges the operation of PDSs. Many issues have arisen, such as lager peak-to-valley differences as well as power quality concerns related to frequency and voltage [8]. To face these challenges, utility planners intend to consider the worst random charging scenario and reserve excess capacities to maintain the functionality of PDSs. As a result, inefficient resource duplication becomes inevitable when the reserved capacities become more than what EVs actually need. Therefore, it is of great importance for PDSs to accurately estimate the charging demand of EVs/FCSs to accommodate EV integration and reduce costs in the planning phase.

In this context, some researchers have already worked on the holistic planning of integrated FCSs and PDSs [9]-[10] Ref. [9] attempts to balance the competing objectives of minimizing the cost and maximizing the serving ranges of FCSs. Considering the EVs as components of the traffic network, a classical approach in transportation, i.e., the user-equilibrium model [11], is employed to simulate traffic flows in [9]. Similarly, ref. [10] utilizes the stochastic traffic assignment model to simulate realistic traffic flows as the basis of multi-objective collaborative planning. However, in terms of integrating simulated traffic flows and EV charging loads, existing assignment models still have two major drawbacks that remain to be addressed:

- Existing traffic models cannot effectively model the impacts of FCSs on traffic flows and EV charging loads. Judging from the formulas of existing models, the impacts of fast/slow charging devices are not properly modeled nor integrated. In other words, existing models are not designed for the EV-integrated traffic flow simulation. To overcome this shortcoming, some studies such as [9]-[11] estimated charging loads statistically based on the simulated traffic flow, which is not reasonable. In fact, the EV charging requirement is associated with its driving behavior, thus they should not be separately considered. Unfortunately, as far as the authors are concerned, the inherent connection between traffic flows and EV charging loads has not been comprehensively modeled.
- Existing joint approaches [9]-[11] failed to reveal the impacts of FCS planning on traffic flows. Thus, installing FCSs on crowded roads is always preferred in existing studies to capture the maximum traffic flow and feed the highest charging demands. However, this will result in more EVs to gather on crowded roads to look for charging services, which in turn worsens the traffic conditions. In addition, existing methods further eliminate the possibility of exploring the potential value of FCS investment in improving traffic conditions.

In summary, a new traffic assignment model is needed to reveal the impacts of FCS planning on traffic flows and integrate the simulations of traffic flows and EV charging loads.

To address the aforementioned issues, studies on microscopic traffic flow assignment can offer a new feasible way. The *microscopic* means that traffic flows are obtained as the output of individual driving analyses, rather than a global variable. At present, there are three popular microscopic models, namely car-following [12], cellular-automata [13], and multi-agent [14]. Among them, the multi-agent model received extensive attention thanks to its mechanism that each agent should dynamically learn from and respond to its surroundings. This mechanism makes it easier to inflect EV/agent driving path with its state of charge (SOC), traffic conditions, siting and sizing of FCSs, and other surrounding information. Different driving paths contribute to the changes in traffic flows, from which the relationship between FCSs and traffic flows can be built. Thus, multi-agent models are commonly reported to handle the charging behaviors of EV/agent [15]. However, such multi-agent methods are generally non-convex and complicated to solve, making them applicable to operation and scheduling problems only. For the studied joint planning problems where integer variables are inevitable, it is of great importance to propose an efficient multi-agent method.

To respond to the mentioned necessities in integrating planning of PDSs and FCSs as well as developing traffic assignment models, a novel joint planning approach is proposed in this paper. First of all, a multi-agent-based microscopic traffic assignment model (MMTAM) is proposed to reveal the inherent connections between traffic flows and EV charging loads. On top of it, a multi-objective joint planning model is developed, in which the non-monetary index (unbalanced traffic flows) and monetary index (i.e., installation costs, operation costs, and power loss costs) are minimized as two separate objectives. Different from traditional approaches such as [9]-[10], two extra obstacles are identified: i) how to obtain a trade-off between different objectives, and ii) how to deal with the non-convexity caused by MMTAM.

For the first obstacle, there are several algorithms available, e.g., the weighted-sum [16], Tchebycheff [17], and non-dominated sorting genetic algorithm II (NSGA-II) [18]. However, all these algorithms have their defects in solving the joint planning model that is generally presented as a mixed-integer

This article has been accepted for publication in a future issue of this journal, but has not been fully edited. Content may change prior to final publication. Citation information: DOI 10.1109/TII.2020.2995742, IEEE Transactions on Industrial Informatics

nonlinear programming (MINLP) problem [9]. For instance, weighted-sum and Tchebycheff are to be blamed for their poor performances in finding the optimal solution while NSGA-II tends to have a heavy computational burden. According to [19]-[20], the general Benders decomposition is effective in solving MINLP problems, but it can not handle multiple objectives. Thus, a bilayer expanded Benders algorithm is developed in this paper to solve the multi-objective optimization. Meanwhile, the proposed algorithm decouples the non-convex MMTAM into different sub-problems to improve computational efficiency, which also tackles the second obstacle.

In summary, the main contributions of this paper are:

- The MMTAM is proposed to make traffic flows and EV charging loads sensitive to FCS planning schemes, which differ from traditionally isolated simulations and lays a foundation for improving traffic conditions by installing new FCSs.
- A multi-objective planning model is developed to balance the interests of PDSs and traffic networks, which addresses the traffic concerns caused by traditional planning approaches.
- A bilayer algorithm is developed to apply Benders decompositions in multi-objective problems, which performs well in improving solving efficiency and robustness.

The rest of this paper is organized as follows. MMTAM approach is presented in Section II. The multi-objective joint planning model is established in Section III. The bilayer expanded Benders algorithm and case studies are respectively proposed in Sections IV and V. Finally, conclusions are given in Section VI.

II. Models for the MMTAM

A. MMTAM Framework and Agent Model

The proposed MMTAM contains three basic layers in its simulation framework, i.e., the geographic layer, agent decision layer, and simulation control layer. The functions of these three layers and mutual data interactions are described in Fig. 1.

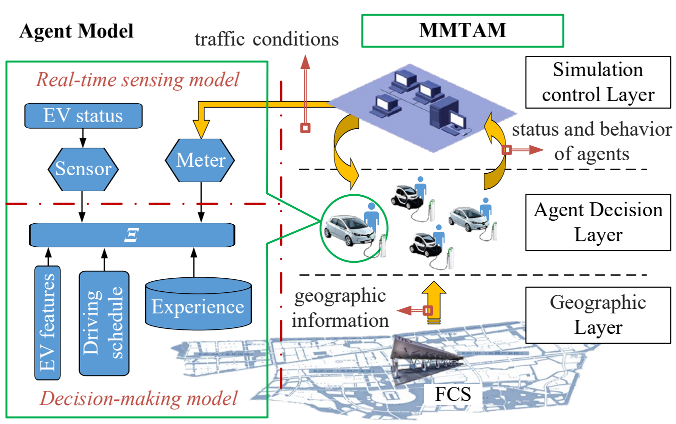

Fig. 1. MMTAM framework and the involved agent model.

In Fig. 1, the simulation control layer acts as a commander, which responsible for collecting data and calculating/broadcasting traffic conditions. Note that *traffic conditions* consist of traffic flows ($F_{ij,t\text{-}1}$) and the average waiting time of FCSs. The geographic layer provides basic geographic information, which includes the locations of agents/FCSs and traffic network topologies. The agent decision layer is the core part of the MMTAM, where all agents optimize their driving paths and schedule charging time via geographic information and traffic conditions.

In the agent decision layer, each agent consists of two sub-models, i.e., the real-time sensing model and the decision-making model. The real-time sensing model gathers essential real-time data such as geographical location and current SOC status and processes the data for decision-making. The decision-making model combines real-time data and other relevant information such as driving schedules and EV features to simulate driver behaviors.

In this process, the decision set $\boldsymbol{\Xi}$={A-1, A-2, A-3, A-4} plays a significant role. Detailed modeling of $\boldsymbol{\Xi}$ will be presented later. Further point-to-point explanations about how to reflect agent features [14]-[15] in the MMTAM are presented in Table I.

TABLE I
EXPLANATIONS ABOUT HOW TO REFLECT TYPICAL AGENT FEATURES

Feature	Description	Way to reflect
Autonomy	make decisions independently	No commander exist in the MMTAM and each EV/agent can decide its behaviors
Reactive	respond to different surroundings	Dynamically update surrounding information and optimize path at each time slot t
Proactive	proactive learning and responding	EV/agent is modeled to minimize its driving cost in the proposed decision set $\boldsymbol{\Xi}$
Social	associate with other agents	State sensing layer acts as the medium of communication, where agents learn from others and work together to reach equilibrium assignment [11]

B. Module A-1: Dynamic Optimal Path Searching

Before a trip, an agent should decide where to go, i.e., select their origin-destination pair [5]-[10]. As soon as the pair is selected, the agent should optimize its path to obtain the lowest driving-cost. To this end, an effective path searching method, i.e., the Bellman-Ford algorithm [21] is implemented. Firstly, each road should be weighted by the function of the Bureau of Public Roads (BPR) [9]-[10], as shown in (2). Then, the *shortest path* will be obtained via the weight matrix ($\boldsymbol{W}_t$) and BPR function. Since considerations of road length and crowded degree, the obtained shortest path refers to a multi-meaning distance called the *link performance distance*:

$$W_{ij,t}=\begin{cases} p_{ij,t\text{-}1} & ij\in\Omega^{\mathrm{TR}} \\ \infty & ij\notin\Omega^{\mathrm{TR}} \end{cases} \tag{1}$$

$$p_{ij,t\text{-}1}=L_{ij}\left[1+\chi\left(F_{ij,t\text{-}1}/c_{ij}\right)^4\right]/v_{ij}^0 \tag{2}$$

$$F_{ij,t\text{-}1}=\sum\nolimits_{k\in\Omega^{\mathrm{AG}}}\sum\nolimits_{ij\in\Omega^{\mathrm{TR}}}\xi_{k,ij,t\text{-}1}/\eta^{\mathrm{AG}} \tag{3}$$

where $W_{ij,t}$ is the element of $\boldsymbol{W}_t$, and $W_{ij,t}$=$p_{ij,t\text{-}1}$ when $ij\in\Omega^{\mathrm{TR}}$, else $W_{ij,t}$=∞; $\xi_{k,ij,t\text{-}1}$ is the binary constant that marks whether road ij is selected in the shortest path of agent k ($\xi_{k,ij,t\text{-}1}$=1) or not ($\xi_{k,ij,t\text{-}1}$=0); χ is the parameter of the BPR function and is set to 0.15 in [9].

In module A-1, it is assumed that agents should dynamically correct their driving paths via updated traffic conditions at each new time slot t. Thus, agents can avoid crowded roads, save waiting time, and decrease driving costs. Learning and reflecting surrounding information (or traffic conditions) belong to typical agent features, i.e., *social* and *reactive*, as described in Table I.

C. Module A-2: Charging Behavior and Navigation

Charging behavior is regarded as an important feature that makes EVs different from traditional fossil fuel vehicles. To analyze the impacts of charging behavior (or FCSs) on traffic flow assignments, the SOC and charging status of agents must be marked during a given driving process. Therefore, an SOC working area is proposed to determine whether or not an EV/agent can finish its driving plan without charging, as illustrated in Fig. 2.

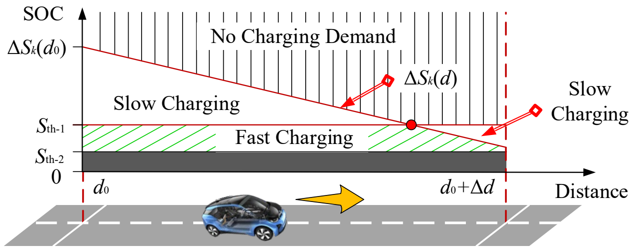

Fig. 2. SOC working area of the agents.

In Fig. 2, the initial mileage of agent k is d_0 and its minimum required SOC is assumed to be a linearly decreasing function $\Delta S_k(d)$, which coincides with the measured "SOC-mileage" relationship [22]. Note that $d\in[d_0, d_0+\Delta d]$ denotes the available mileage. As the EV approaches its destination, a lower minimum SOC $\Delta S_k(d)$ is required to finish the trip without charging.

When an EV cannot finish the trip while maintaining its lowest SOC threshold $S_{\text{th-2}}$, the EV/agent in Fig. 2 has to find an FCS to do the emergency charging. It is assumed that the EV/agent prefers the fast charging service so that the vehicle can route to its destination as soon as possible. Otherwise, EVs/agents tend to do slow charging after finishing their trips. Thus, during the driving process, traffic flows will only be influenced by the fast charging behaviors of EVs in this paper.

Equation (4) can be derived to describe Fig. 2:

$$\lambda_{k,t}=\begin{cases}1 & \text{if } S_{\text{th-2}}\le S_{k,t}<\min\{S_{\text{th-1}},\Delta S_k(d)\}\\ 0 & \text{if } \min\{S_{\text{th-1}},\Delta S_k(d)\}\le S_{k,t}<\max\{S_{\text{th-1}},\Delta S_k(d)\}\\ -1 & \text{if } S_{k,t}\ge\max\{S_{\text{th-1}},\Delta S_k(d)\}\end{cases} \quad (4)$$

where $\lambda_{k,t}=\{1, 0, -1\}$ respectively denote that fast, slow, or no charging is needed for the corresponding agent.

When $\lambda_{k,t}=1$, agent k needs to charge its EV to finish its trip, but its optimal path may not necessarily include any FCS. In that case, the path of agent k should change. To this end, a charging model has been proposed to select the optimal FCS and offer a navigation service [23] for the agents, as formulated below:

$$\min \quad f_{k,t}^{\text{RID}}=\psi_{\text{BFA}}\left(O_{k,t},\textstyle\sum_{q\in\Omega^{\text{FCS}}}\varepsilon_{k,q,t}D_q\right) \quad (5)$$

$$\text{s.t.} \quad \textstyle\sum_{q\in\Omega^{\text{FCS}}}\varepsilon_{k,q,t}=1; \quad \sum_{q\in\Omega^{\text{FCS}}}\varepsilon_{k,q,t}t_{q,t\text{-}1}^{\text{aver}}\le\bar{t}_k \quad (6)$$

$$f_{k,t}^{\text{RID}}\le 100\left(S_{k,t}\text{-}S_{\text{th-2}}\right)C_k^{\text{AG}}/E_k^{\text{AG}} \quad (7)$$

where $\varepsilon_{k,q,t}$ is the binary variable that denotes whether the FCS q is selected by agent k ($\varepsilon_{k,q,t}$=1) or not ($\varepsilon_{k,q,t}$=0). $\psi_{\text{BFA}}(\bullet)$ denotes the Bellman-Ford algorithm that used to search the shortest link performance distance between $O_{k,t}$ and $\varepsilon_{k,q,t}D_q$ (only when $\varepsilon_{k,q,t}$=1).

Equation (6) ensures that only one FCS that meets the agent's waiting time requirement will be selected. In Equation (7), the selected FCS must be within the mileage range of the agent according to its current SOC and the traffic network information.

The fast charging behavior further leads to an update of $\xi_{k,ij,t\text{-}1}$ (obtained by $\psi_{\text{BFA}}(\bullet)$ and varied with different driving paths) and the traffic flow $F_{ij,t\text{-}1}$ according to (3). In this way, module A-2 can mathematically calculate the impacts of FCSs (or agents' charging behaviors) on the traffic flow assignment.

D. Module A-3: Circular Departing Mechanisms

In the MMTAM, each EV/agent is marked with three kinds of trip-chains [25], i.e., the timing chain, SOC chain, and location chain. Different from traditional trip-chain based methods [25], MMTAM respects the multi-trip behavior of EVs/agents by processing circular departing mechanisms. There are two types of EVs, i.e., the private car and taxi, are studied via their unique driving behaviors, as analyzed in [15], [24]-[25]. Detailed mechanism descriptions are omitted here due to the limited space.

E. Module A-4: Fast and Slow Charging Loads

The fast-charging load of FCS q is calculated based on the number of agents whose "$\lambda_{k,t}$=1", as shown below:

$$P_{q,t}^{\text{FCS}}=\min\left\{n_q^{\text{FC}}P^{\text{FC}},n_{q,t}^{\text{FAG}}P^{\text{FC}}\right\} \quad \forall q\in\Omega^{\text{FCS}},\forall t\in\mathrm{T} \quad (8)$$

Meanwhile, considering the benefits of ordered slow charging in [8] and [26], e.g., reducing peak-to-valley differences, consuming more renewable energies, etc., a variable $\beta_{u,k,t}$ is used to simulate the agents' expectation of taking part in slow charging management, as follows:

$$P_{u,t}^{\text{CP}}=\min\left\{n_u^{\text{SC}}P^{\text{SC}},n_{u,t}^{\text{SAG}}\beta_{u,k,t}P^{\text{SC}}\right\} \quad \forall u\in\Omega^{\text{B}},\forall k\in\Omega^{\text{AG}},\forall t\in\mathrm{T} \quad (9)$$

In (9), the slow charging load $P_{u,t}^{\text{CP}}$ depends on both the charging status ($\lambda_{k,t}$=0) and variable $\beta_{u,k,t}$ that involves driving schedule, payment, and available locations, as described in [27]. It is assumed that $\beta_{u,k,t}$=1 when the expectation of slow charging higher than 50%; otherwise, $\beta_{u,k,t}$=0.

F. MMTAM Nonlinear Function

With the decision-making set $\boldsymbol{\Xi}$={A-1, A-2, A-3, A-4} modeled, the proposed MMTAM can be corded in the MATLAB-2014b platform [28] to simulate daily traffic flows and EV charging loads from 0:00 to 24:00, as shown in Fig. 3.

To conveniently apply the MMTAM in the joint planning problem, the MMTAM is modulated as a nonlinear function $\psi_{\text{MMTAM}}(\bullet)$. Note that $\psi_{\text{MMTAM}}(\bullet)$ cannot be explicitly formulated and shows high non-convexity. Thus, only a brief input & output form is presented, as given below:

$$[\boldsymbol{F}^{\tau},\boldsymbol{P}^{\text{FCS},\tau},\boldsymbol{P}^{\text{CP},\tau}]=\psi_{\text{MMTAM}}(\boldsymbol{x}^{\tau},\boldsymbol{N}^{\tau},\Omega^{\text{FCS},\tau}) \quad \forall\tau\in\Gamma \quad (10)$$

where $\boldsymbol{x}^{\tau}$ is the binary variable matrix that denotes whether a candidate position of FCSs is selected at stage τ ($\boldsymbol{x}^{\tau}$=$\boldsymbol{I}$) or not ($\boldsymbol{x}^{\tau}$=$\boldsymbol{0}$); and $\boldsymbol{N}^{\tau}$ means the optimal installed number of fast-charging devices at stage τ.

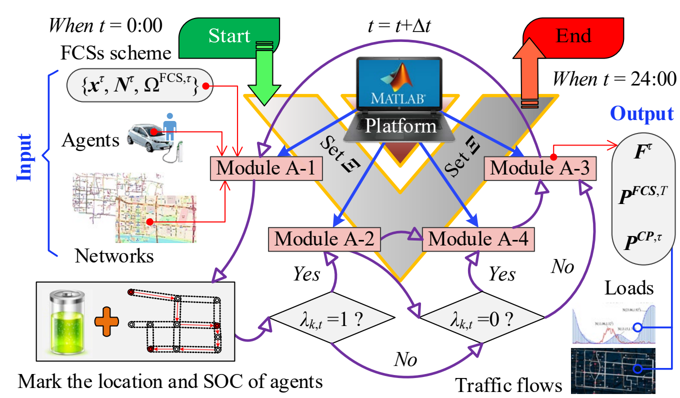

Fig. 3. Flowchart of the MMTAM.

As mentioned in module A-2, agents should change the current driving paths to charge EVs via the siting and sizing of FCSs when $\lambda_{k,t}$=1. Different driving paths contribute to the changes in traffic flows, from which the relationship between FCSs and traffic flows/charging loads can be built. That is, the output matrix $\{\boldsymbol{F}^{\tau},\boldsymbol{P}^{\text{FCS},\tau},\boldsymbol{P}^{\text{CP},\tau}\}$ in (10) is supposed to be influenced with different planning scheme or input data $\{\boldsymbol{x}^{\tau},\boldsymbol{N}^{\tau},\Omega^{\text{FCS},\tau}\}$. This feature makes the traffic simulation sensitive to different schemes and can be applied in joint planning

TABLE II
DIFFERENCES BETWEEN THE MMTAM AND EXISTING RELATIVE METHODS

Methods: Category	Methods: Theory	References	Functions list: Consider traffic network	Fast charging simulation	Slow charging simulation	Traffic flow assignment	Impacts of FCSs	Charging navigation	Adapt to joint planning
EV charging loads simulation	Monte Carlo	[22]	×	×	√	×	×	×	×
EV charging loads simulation	Trip-chain	[25]	√	×	√	×	×	×	×
Traffic flow Assignment – Macroscopic	User-equilibrium	[9]	√	×	×	√	×	×	√
Traffic flow Assignment – Microscopic	Multi-agent	[14]	√	×	×	√	×	×	×
Traffic flow Assignment – Microscopic	Cellular-automata	[13]	√	√	×	√	√	√	×
Proposed MMTAM	Multi-agent	--	√	√	√	√	√	√	√

* Symbol "√" means the method has this function; otherwise, it is marked with "×".

problems. In any iteration of a planning process, all candidate schemes should be processed by (10) to obtain the corresponding outputs, which will then be used as the basis for further optimization.

To highlight the contributions of MMTAM, Table II compares the proposed MMTAM with other existing relative methods in detail. It is concluded that MMTAM is a more functional and comprehensive approach, which unit the existing methods of the EV load simulation [22], [25] and traffic flow assignment [9], [13], [14]. Its effectiveness will be validated in case studies.

III. MULTI-OBJECTIVE JOINT PLANNING MODEL

A. Unbalance of Traffic Flow Assignment

Apart from the commonly used economic objective, i.e., installation & operation costs (f^{FCS}), the positive role of FCSs in balancing the traffic flow assignment also deserves more attention. In general, the traditional planning approach prefers to install FCSs on the crowded roads to feed more charging demands. As a consequence, more EVs will be attracted to charge at roads with heavy traffic, which further worsens the traffic condition.

To handle this problem, a variance indicator $\rho(\cdot)$ is proposed to evaluate the unbalance of the traffic flow assignment. As shown in (11), $\rho(\cdot)$ is calculated by comparing the ratio of traffic flow to capacity with the equilibrium value α. Note that $\alpha\in[0,1]$ is set to a constant based on the assumption that all roads remain at the same ratio of traffic flow to capacity when the assignment reaches an equilibrium [11]. The traffic flow unbalances of road ij at time t, i.e., $\Re(\cdot)$, is calculated in (12).

$$\rho(\omega)=\left(\omega/c_{ij}-\alpha\right)^2 \tag{11}$$

$$\Re\left(F_{ij,t}^{\tau}\right)=\int_0^{F_{ij,t}^{\tau}}\rho(\omega)\,d\omega=F_{ij,t}^{\tau\,3}/\left(3c_{ij}^{\,2}\right)-\alpha F_{ij,t}^{\tau\,2}/c_{ij}+\alpha^2F_{ij,t}^{\tau} \tag{12}$$

where ω denotes the differential variable of traffic flows, which takes value from $[0, F_{ij,t}^{\tau}]$.

Considering the indicator $\rho(\cdot)$ varies with ω, the unbalance $\Re(\cdot)$ is calculated as the integration of $\rho(\cdot)$ to reflect a changing ω, as shown in (12).

B. Planning of FCSs

As discussed in Section III.A, the planning of FCSs should consider both traffic flow unbalances and FCS installation & operation costs. Because the unbalance $\Re(\cdot)$ cannot be directly evaluated in monetary terms, two sub-objectives are preferably formulated as follows:

$$\min \quad f^{\mathrm{UB}}=\sum\nolimits_{t\in\mathrm{T}}\left(1/N^{\mathrm{TR}}\right)\sum\nolimits_{ij\in\Omega^{\mathrm{TR}}}\Re\left(F_{ij,t}^{\tau}\right) \tag{13}$$

$$\min \quad f^{\mathrm{FCS}}=\sum\nolimits_{\tau\in\Gamma}(1+\gamma)^{-\tau}\sum\nolimits_{q\in\Omega^{\mathrm{FCS},\tau}}x_q^{\tau}N_q^{\tau}\left(\mu^{\mathrm{F},\tau}+\kappa^{\mathrm{F},\tau}+\delta_q^{\mathrm{F},\tau}\right) \tag{14}$$

where x_q^{τ} is the element of matrix $\boldsymbol{x}^{\tau}$; N^{TR} denotes the number of traffic roads; and N_q^{τ} means the number of fast-charging devices installed in FCS q at stage τ, which is limited to $[\underline{N}, \overline{N}]$.

In (13), sub-objective f^{UB} is set as the average unbalance of all traffic roads in a day around. Cost f^{FCS} in (14) depends on the installed number of fast-charging devices, which has been discounted to the current planning year.

The constraints of the FCS planning model include:

$$\sum\nolimits_{q\in\Omega^{\mathrm{FCS},\tau}}x_q^{\tau}\geq\underline{n}^{\mathrm{FCS},\tau};\quad \sum\nolimits_{\tau\in\Gamma}x_q^{\tau}\leq1 \quad \forall q\in\Omega^{\mathrm{FCS},\tau} \tag{15}$$

$$x_q^{\tau}\underline{N}\leq x_q^{\tau}N_q^{\tau}\leq x_q^{\tau}\overline{N} \quad \forall q\in\Omega^{\mathrm{FCS},\tau} \tag{16}$$

$$\boldsymbol{F}^{\tau}=\psi_{\mathrm{MMTAM}}\left(\boldsymbol{x}^{\tau},\boldsymbol{N}^{\tau},\Omega^{\mathrm{FCS},\tau}\right) \quad \forall\tau\in\Gamma \tag{17}$$

In (15), the first formula shows that the installed number of FCSs should not be less than a certain amount (i.e., $\underline{n}^{\mathrm{FCS},\tau}$), which reflects the influence of governmental efforts to popularize EVs; and, the second constraint ensures that each candidate FCS will be installed at most once. The relaxed numerical constraints of N_q^{τ} is presented in (16). Equation (17) shows that $F_{ij,t\text{-}1}^{\tau}/\boldsymbol{F}^{\tau}$ is obtained by the aforementioned function $\psi_{\mathrm{MMTAM}}(\cdot)$, as introduced in Section II.F.

C. Planning of PDSs

The planning of PDSs is a mature research topic and many referable models are available [9]-[10], [29]. Based on these studies, this paper respectively minimizes the feeder installation costs ($f^{\mathrm{F},\tau}$) and transformer installation/reinforcement & operation costs ($f^{\mathrm{B},\tau}$). In addition, as an important indicator of the economic operation, power loss costs ($f^{\Delta,\tau}$) should also be considered during the planning stage. With the well-established Distflow equations as constraints [30], the planning model of PDSs can be mathematically described as:

$$\min \quad f^{\mathrm{PDS}}=\sum\nolimits_{\tau\in\Gamma}(1+\gamma)^{-\tau}\left(f^{\mathrm{F},\tau}+f^{\Delta,\tau}+f^{\mathrm{B},\tau}\right) \tag{18}$$

$$\text{s.t.} \quad f^{\mathrm{F},\tau}=\sum\nolimits_{u\in\Omega^{\mathrm{PB},\tau}}\sum\nolimits_{a\in\Omega^{\mathrm{F},\tau}}c_{u,a}^{\tau}\,y_{u,a}^{\tau}\,l_{u,a}^{\tau} \tag{19}$$

$$\begin{aligned} f^{\Delta,\tau}\geq&\left(\sigma d^{\mathrm{A}}\Delta t/V_{\mathrm{B}}^{\,2}\right)\sum\nolimits_{t\in\mathrm{T}}\sum\nolimits_{u\in\Omega^{\mathrm{EB},\tau}}\left(P_{u,t}^{\tau\,2}+Q_{u,t}^{\tau\,2}\right)R_u^{\tau} \\ &+\left(\sigma d^{\mathrm{A}}\Delta t/V_{\mathrm{B}}^{\,2}\right)\sum\nolimits_{t\in\mathrm{T}}\sum\nolimits_{u\in\Omega^{\mathrm{PB},\tau}}\left(P_{u,t}^{\tau\,2}+Q_{u,t}^{\tau\,2}\right)\sum\nolimits_{a\in\Omega^{\mathrm{F},\tau}}y_{u,a}^{\tau}R_{u,a}^{\tau} \end{aligned} \tag{20}$$

$$f^{\mathrm{B},\tau}=\left(\mu^{\mathrm{B},\tau}+\kappa^{\mathrm{B},\tau}+\delta^{\mathrm{B},\tau}\right)\sum\nolimits_{b\in\Omega^{\mathrm{S},\tau}}\left(\sum\nolimits_{u\in\Omega^{\mathrm{PB},\tau}}S_{u,b}^{\tau}z_{u,b}^{\mathrm{P},\tau}+\sum\nolimits_{u\in\Omega^{\mathrm{EB},\tau}}S_{u,b}^{\tau}z_{u,b}^{\mathrm{E},\tau}\right) \tag{21}$$

$$\sum\nolimits_{v\in\Omega^{\mathrm{PB},\tau}\cup\Omega^{\mathrm{EB},\tau}}A_{u,v}^{\tau}P_{u,t}^{\tau}=P_{u,t}^{\mathrm{L},\tau}\text{-}P_{u,t}^{\mathrm{S},\tau}+\left(x_q^{\tau}\,\varphi_{q,u}^{\tau}\,P_{u,t}^{\mathrm{FCS},\tau}+P_{u,t}^{\mathrm{CP},\tau}\right) \tag{22}$$

$$\sum\nolimits_{v\in\Omega^{\mathrm{PB},\tau}\cup\Omega^{\mathrm{EB},\tau}}A_{u,v}^{\tau}Q_{u,t}^{\tau}=Q_{u,t}^{\mathrm{L},\tau}-Q_{u,t}^{\mathrm{S},\tau} \tag{23}$$

$$\sum\nolimits_{v\in\Omega^{\mathrm{PB},\tau}\cup\Omega^{\mathrm{EB},\tau}}A_{u,v}^{\tau}V_{u,t}^{\tau}=\left(R_u^{\tau}P_{u,t}^{\tau}+X_u^{\tau}Q_{u,t}^{\tau}\right)/V_{\mathrm{B}} \tag{24}$$

$$\underline{V}\leq V_{u,t}^{\tau}\leq\overline{V} \quad \forall u\in\Omega^{\mathrm{PB},\tau}\cup\Omega^{\mathrm{EB},\tau} \tag{25}$$

$$\sqrt{P_{u,t}^{\tau\,2}+Q_{u,t}^{\tau\,2}}\leq\sum\nolimits_{b\in\Omega^{\mathrm{S},\tau}}S_{u,b}^{\tau}z_{u,b}^{\mathrm{P},\tau} \quad \forall u\in\Omega^{\mathrm{PB},\tau} \tag{26}$$

$$\sqrt{P_{u,t}^{\tau\,2}+Q_{u,t}^{\tau\,2}}\leq S_u^{0,\tau}+\sum\nolimits_{b\in\Omega^{\mathrm{S},\tau}}S_{u,b}^{\tau}z_{u,b}^{\mathrm{E},\tau} \quad \forall u\in\Omega^{\mathrm{EB},\tau} \tag{27}$$

$$\sum\nolimits_{\tau\in\Gamma}\sum\nolimits_{a\in\Omega^{\mathrm{F},\tau}}y_{u,a}^{\tau}=1;\quad \sum\nolimits_{\tau\in\Gamma}\sum\nolimits_{b\in\Omega^{\mathrm{S},\tau}}z_{u,b}^{\mathrm{P},\tau}=1 \quad \forall u\in\Omega^{\mathrm{PB},\tau} \tag{28}$$

$$\sum\nolimits_{b\in\Omega^{\mathrm{S},\tau}}z_{u,b}^{\mathrm{E},\tau}\leq1 \quad \forall u\in\Omega^{\mathrm{EB},\tau},\ \forall\tau\in\Gamma \tag{29}$$

$$x_q^{\tau}=\sum\nolimits_{u\in\Omega^{\mathrm{PB},\tau}\cup\Omega^{\mathrm{EB},\tau}}\varphi_{q,u}^{\tau} \quad q\in\Omega^{\mathrm{FCS},\tau},\ \forall\tau\in\Gamma \tag{30}$$

$$\left[\boldsymbol{P}^{\mathbf{FCS},\tau},\boldsymbol{P}^{\mathbf{CP},\tau}\right]=\psi_{\mathrm{MMTAM}}\left(\boldsymbol{x}^{\tau},\boldsymbol{N}^{\tau},\Omega^{\mathrm{FCS},\tau}\right) \quad \forall\tau\in\Gamma \tag{31}$$

where $A_{u,v}$ is the element of the directed adjacent matrix, i.e., $A_{u,v}=\pm1$ when the buses (u, v) are linked, otherwise $A_{u,v}=0$.

This article has been accepted for publication in a future issue of this journal, but has not been fully edited. Content may change prior to final publication. Citation information: DOI 10.1109/TII.2020.2995742, IEEE Transactions on Industrial Informatics

The objective function (18) minimizes the total planning cost f^{PDS}, whose components are calculated through (19)-(21), respectively. Among them, $f^{\text{F},\tau}$ in (19) is calculated with the length and unit cost of candidate feeders. Power loss $f^{\Delta,\tau}$ is approximated by (20), which is commonly used in existing works [30]. Equation (21) calculates the costs of installing/reinforcing transformers, i.e., $f^{\text{B},\tau}$, via its unit costs $\{\mu^{\text{B},\tau}, \kappa^{\text{B},\tau}, \delta^{\text{B},\tau}\}$.

Constraints (22)-(27) are derived from Distflow equations, which are respectively the active/reactive power balance equation, the voltage drop calculation formula, the voltage amplitude constraint, and the transformer capacity constraint. Equation (28) ensures that candidate feeders and buses are installed only once. The reinforcement time of existing buses during a planning stage is limited in (29). Constraint (30) links variables x_q^τ and $\varphi_{q,u}^\tau$, i.e, candidate FCS q can choose a bus to contact by $\varphi_{q,u}^\tau$ only when x_q^τ=1. Equation (31) indicates that both fast and slow EV charging loads are obtained from the proposed MMTAM.

Note that the power loss is approximated by a relaxed form shown in (20) to guarantee the convexity of the power flow constraints. This approximation has been validated by studies such as [30] and is not discussed further due to space limitations.

D. Joint Planning Model for Integrated FCSs and PDSs

Two sub-objectives (f_1 and f_2) are established via the FCS planning model in Section III.B and the PDS planning model in Section III.C, respectively. Because f^{UB} is not a monetary index, it cannot be directly combined with f^{FCS} in f_1. Similarly, f_1 and f_2 also cannot be directly added. Thus, the joint planning model for the integrated FCSs and PDSs, denoted as M-0, should be formulated as a multi-objective optimization model, expressed as:

M-0:

$$\begin{aligned} \min\quad & \{f_1 = f^{\text{UB}}\ ;\ f_2 = f^{\text{FCS}} + f^{\text{PDS}}\} \\ \text{s.t.}\quad & (12), (15)\text{-}(17), (19)\text{-}(31) \end{aligned}$$

The proposed model M-0 is a multi-objective MINLP problem with nonlinear sub-objective f^{UB} and highly non-convex constraints such as $\psi_{\text{MMTAM}}(\bullet)$. In other words, model M-0 cannot be directly solved by commercial solvers. In this regard, a new algorithm is proposed to solve model M-0 in a decoupled fashion, as will be discussed in the next section.

IV. A Bilayer Expanded Benders Decomposition

To solve the proposed multi-objective MINLP model M-0, a bilayer expanded algorithm is proposed via the idea of classical general Benders decompositions.

A. Algorithm Description

Similar to the classical Benders theory, our algorithm requires M-0 to be decomposed into two kinds of sub-problems, i.e., master problems and slave problems. However, the difference is, here we generate two pairs of "master-slave" subproblems, i.e., {M-1, M-S1} and {M-2, M-S2}, to handle the coupling between two objectives (f_1 and f_2) of the proposed M-0. Each "master-slave" pair aims at optimizing a single objective. The sub-problems M-1, M-2, M-S1, and M-S2 are respectively described as follows:

M-1:

$$\begin{aligned} \min\quad & f_{1,\text{M-1}}^{(h,m)} \\ \text{s.t.}\quad & f_{\text{M-1}}^{\text{FCS}(h,m)} \le (1-\theta) f_{\text{M-1}}^{\text{FCS}(h,m\text{-}1)} + \theta f_{\text{M-S1}}^{\text{FCS}(h,m\text{-}1)} \\ & (12), (16)\text{-}(17), (31) \end{aligned} \tag{32}$$

M-2:

$$\begin{aligned} \min\quad & f_2^{(h,m)} = f^{\text{C},\tau(h,m)} + \beta_1^{(h,m)} + \beta_2^{(h,m)} \\ \text{s.t.}\quad & f^{\text{C},\tau(h,m)} = \textstyle\sum_{\tau\in\Gamma} (1+\gamma)^{-\tau} \left(f^{\text{F},\tau(h,m)} + f^{\text{B},\tau(h,m)}\right) \\ & f_{\text{S1}}^{(h,m)} + B_{\text{cut1}}^{(h,m)} \le \beta_1^{(h,m)};\quad f_{\text{S2}}^{(h,m)} + B_{\text{cut2}}^{(h,m)} \le \beta_2^{(h,m)} \\ & f_{\text{V}}^{(h,m)} + B_{\text{cut3}}^{(h,m)} \le 0;\quad (15), (28)\text{-}(30) \end{aligned} \tag{33}$$

M-S1:

$$\begin{aligned} \min\quad & f_{\text{S1}}^{(h,m)} = f_{\text{M-S1}}^{\text{FCS}(h,m)} \\ \text{s.t.}\quad & f_{1,\text{M-S1}}^{(h,m)} \le (1-\theta) f_{1,\text{M-1}}^{(h,m\text{-}1)} + \theta f_{1,\text{M-S1}}^{(h,m\text{-}1)} \\ & (12), (16)\text{-}(17), (31) \end{aligned} \tag{34}$$

M-S2:

$$\begin{aligned} \min\quad & f_{\text{S2}}^{(h,m)} = \textstyle\sum_{\tau\in\Gamma} (1+\gamma)^{-\tau} f^{\Delta,\tau} \\ \text{s.t.}\quad & \boldsymbol{P}_{\text{M-S2}}^{\textbf{FCS},\tau(h,m)} = \boldsymbol{P}_{\text{M-S1}}^{\textbf{FCS},\tau(h,m)};\quad \boldsymbol{P}_{\text{M-S2}}^{\textbf{CP},\tau(h,m)} = \boldsymbol{P}_{\text{M-S1}}^{\textbf{CP},\tau(h,m)} \\ & (19)\text{-}(27) \end{aligned} \tag{35}$$

where $f^{\text{C},\tau(h,m)}$ denotes the installation cost at stage τ; $f_{1,\text{M-1}}^{(h,m)}$ ($f_{\text{M-1}}^{\text{FCS}(h,m)}$) and $f_{1,\text{M-S1}}^{(h,m)}$ ($f_{\text{M-S1}}^{\text{FCS}(h,m)}$) are respectively the optimal objective f_1 (f^{FCS}) of models M-1 and M-S1; $\theta\in[0,1]$ is the learning factor; $\boldsymbol{P}_{\text{M-S1}}^{\textbf{FCS},\tau(h,m)}$ ($\boldsymbol{P}_{\text{M-S2}}^{\textbf{FCS},\tau(h,m)}$) and $\boldsymbol{P}_{\text{M-S1}}^{\textbf{CP},\tau(h,m)}$ ($\boldsymbol{P}_{\text{M-S2}}^{\textbf{CP},\tau(h,m)}$) respectively denote the optimal $\boldsymbol{P}^{\textbf{FCS},\tau}$ and $\boldsymbol{P}^{\textbf{CP},\tau}$ of M-S1 (M-S2); $f_{\text{S1}}^{(h,m)}$ ($f_{\text{S2}}^{(h,m)}$, $f_{\text{V}}^{(h,m)}$) is the optimal objective of slave problem M-S1 (M-S2, M-V); $B_{\text{cut1}}^{(h,m)}$ ($B_{\text{cut2}}^{(h,m)}$, $B_{\text{cut3}}^{(h,m)}$) denotes the linear Benders cut [19]-[20]; and $\beta_1^{(h,m)}$ and $\beta_2^{(h,m)}$ are both nonnegative variables.

Compared to classical Benders algorithms, more constraints are needed to coordinate two "master-slave" pairs: 1) equations (32) and (34) are newly proposed to reshape the feasible spaces of f_1 and f_2 iteratively; 2) equation (33) uses two variables, i.e., $\beta_1^{(h,m)}\ge 0$ and $\beta_2^{(h,m)}\ge 0$, to constrain the upper limits of Benders cuts, while only one variable is required in the traditional algorithm; and 3) equation (35) is presented to decouple $\psi_{\text{MMTAM}}(\bullet)$ from models M-S2 and M-V to keep them convex.

In any iteration m, {M-1, M-2} are solved first to obtain optimal binary variables $\{\boldsymbol{x}^{(h,m)}, \boldsymbol{y}^{(h,m)}, \boldsymbol{z}^{(h,m)}, \boldsymbol{\varphi}^{(h,m)}\}$, based on which {M-S1, M-S2} are then optimized. Note that, since it represents a simulation method, the function $\psi_{\text{MMTAM}}(\bullet)$ can obtain outputs $\{\boldsymbol{F}^\tau, \boldsymbol{P}^{\textbf{FCS},\tau}, \boldsymbol{P}^{\textbf{CP},\tau}\}$ for any input $\{\boldsymbol{x}^\tau, N_q^\tau\}$, so the feasibility of M-S1 is always guaranteed. In contrast, similar to the general Benders decomposition algorithm, optimal binary variables of M-2 may lead to an infeasible M-S2. In this case, a virtual feasibility slave problem M-V will be solved instead. The M-V model is mathematically described as:

M-V:

$$\begin{aligned} \min\quad & f_{\text{V}}^{(h,m)} = \textstyle\sum_{u\in\Omega^{\text{PB},\tau}\cup\Omega^{\text{EB},\tau}} \left(P_{u,t}^{\text{VS},\tau(h,m)} + P_{u,t}^{\text{VL},\tau(h,m)}\right) \\ \text{s.t.}\quad & \boldsymbol{P}_{\text{M-S2}}^{\textbf{FCS},\tau(h,m)} = \boldsymbol{P}_{\text{M-S1}}^{\textbf{FCS},\tau(h,m)};\quad \boldsymbol{P}_{\text{M-S2}}^{\textbf{CP},\tau(h,m)} = \boldsymbol{P}_{\text{M-S1}}^{\textbf{CP},\tau(h,m)} \\ & \textstyle\sum_{v\in\Omega^{\text{PB},\tau}\cup\Omega^{\text{EB},\tau}} A_{u,v}^\tau P_{u,t}^\tau + P_{u,t}^{\text{VS},\tau(h,m)} = P_{u,t}^{\text{VL},\tau(h,m)} + P_{u,t}^{\text{L},\tau} - P_{u,t}^{\text{S},\tau} + \left(P_{u,t}^{\text{FCS},\tau} + P_{u,t}^{\text{CP},\tau}\right) \\ & (19)\text{-}(21), (23)\text{-}(27), (35) \end{aligned} \tag{36}$$

Equation (36) is the relaxed form of (22) after adding a virtual power source ($P_{u,t}^{\text{VS},\tau(h,m)}\ge 0$) and a virtual load ($P_{u,t}^{\text{VL},\tau(h,m)}\ge 0$) to enforce the feasibility of model M-V.

Benders cuts $\{B_{\text{cut1}}^{(h,m)}, B_{\text{cut2}}^{(h,m)}, B_{\text{cut3}}^{(h,m)}\}$ are formulated as:

$$B_{\text{cut1}}^{(h,m)} = \textstyle\sum_{\tau\in\Gamma} \boldsymbol{\varpi}_1 \sum(\boldsymbol{x} - \boldsymbol{x}^{(h,m)}) \tag{37}$$

$$B_{\text{cut2}}^{(h,m)} = \textstyle\sum_{\tau\in\Gamma} \boldsymbol{\varpi}_2 \bullet [\sum(\boldsymbol{y} - \boldsymbol{y}^{(h,m)}), \sum(\boldsymbol{z} - \boldsymbol{z}^{(h,m)}), \sum(\boldsymbol{\varphi} - \boldsymbol{\varphi}^{(h,m)})]^{\text{T}} \tag{38}$$

$$B_{\text{cut3}}^{(h,m)} = \textstyle\sum_{\tau\in\Gamma} \boldsymbol{\varpi}_3 \bullet [\sum(\boldsymbol{y} - \boldsymbol{y}^{(h,m)}), \sum(\boldsymbol{z} - \boldsymbol{z}^{(h,m)}), \sum(\boldsymbol{\varphi} - \boldsymbol{\varphi}^{(h,m)})]^{\text{T}} \tag{39}$$

where $\boldsymbol{\varpi}_1$, $\boldsymbol{\varpi}_2$ and $\boldsymbol{\varpi}_3$ respectively denote the vectors of the dual multipliers of linear Benders cuts [19]-[20].

As shown in (37)-(39), Benders cuts are updated by summing the differences between historical values $\{\boldsymbol{x}, \boldsymbol{y}, \boldsymbol{z}, \boldsymbol{\varphi}\}$ and current values $\{\boldsymbol{x}^{(h,m)}, \boldsymbol{y}^{(h,m)}, \boldsymbol{z}^{(h,m)}, \boldsymbol{\varphi}^{(h,m)}\}$.

This article has been accepted for publication in a future issue of this journal, but has not been fully edited. Content may change prior to final publication. Citation information: DOI 10.1109/TII.2020.2995742, IEEE Transactions on Industrial Informatics

To solve multi-objective problems, the proposed expanded Benders algorithm consists of outer and inner optimization layers. The outer-layer aims at reducing the error between two objectives f_1 and f_2, whose round number is marked with a superscript (m). In the m-th round of outer-layer optimization, the inner-layer iteratively generates Benders cuts to obtain feasible solutions and minimize costs. The iteration number of the inner-layer within the m-th outer-layer optimization is denoted as $h^{(m)}$. Assuming the outer-layer converges at the $m^{\max}$-th round, the total number of Benders iterations is calculated as $\sum_{m=1}^{m^{\max}} h^{(m)}$. The convergence criteria of inner and outer-layers are respectively presented as:

$$B_{\text{cut1}}^{(h,m)}+B_{\text{cut2}}^{(h,m)}+B_{\text{cut3}}^{(h,m)}=0 \tag{40}$$

$$\frac{\left|f_{\text{1,M-1}}^{(h,m)}-f_{\text{1,M-S1}}^{(h,m)}\right|}{f_{\text{1,M-S1}}^{(0)}-f_{\text{1,M-1}}^{(0)}}+\frac{\left|f_{\text{2,M-1}}^{(h,m)}-f_{\text{2,M-S1}}^{(h,m)}\right|}{f_{\text{2,M-1}}^{(0)}-f_{\text{2,M-S1}}^{(0)}}\leq\omega \tag{41}$$

where ω denotes the acceptable convergence tolerance.

The initial $\{f_{\text{1,M-1}}^{(0)}, f_{\text{2,M-1}}^{(0)}\}$ and $\{f_{\text{1,M-S1}}^{(0)}, f_{\text{2,M-S1}}^{(0)}\}$ are obtained by optimizing M-0 when only one objective, i.e., f_1 or f_2, is considered.

B. Solution Steps

In Section IV.A, the "master-slave" pair {M-1, M-S1} both contain function $\psi_{\text{MMTAM}}(\cdot)$, which is too non-convex to be solved by commercial solvers. Thus, {M-1, M-S1} will be solved through an improved genetic algorithm [29]. The remaining models {M-2, M-S2, M-V} are either integer programming problems or quadratically constrained programming problems, which can be efficiently solved by the YALMIP/CPLEX optimizer [31].

The proposed bilayer expanded Benders algorithm proceeds through an iterative auction process, as described in the following Pseudocode. Note that the outer-layer contains steps 3-17, while the inner-layer contains steps 6-16.

Pseudocode of the Bilayer Expanded Benders Algorithm

Input: θ, ω, $\{f_{\text{1,M-S1}}^{(0)}, f_{\text{2,M-S1}}^{(0)}, f_{\text{1,M-1}}^{(0)}, f_{\text{2,M-1}}^{(0)}\}$

1. $m \leftarrow 0$; $h \leftarrow 0$;
2. $f_{\text{1,M-S1}}^{(h,m)}=f_{\text{1,M-S1}}^{(0)}$; $f_{\text{2,M-S1}}^{(h,m)}=f_{\text{2,M-S1}}^{(0)}$; $f_{\text{1,M-1}}^{(h,m)}=f_{\text{1,M-1}}^{(0)}$; $f_{\text{2,M-1}}^{(h,m)}=f_{\text{2,M-1}}^{(0)}$;
3. **while** $\frac{\left|f_{\text{1,M-1}}^{(h,m)}-f_{\text{1,M-S1}}^{(h,m)}\right|}{f_{\text{1,M-S1}}^{(0)}-f_{\text{1,M-1}}^{(0)}}+\frac{\left|f_{\text{2,M-1}}^{(h,m)}-f_{\text{2,M-S1}}^{(h,m)}\right|}{f_{\text{2,M-1}}^{(0)}-f_{\text{2,M-S1}}^{(0)}}>\omega$ **do**
4. $m \leftarrow m+1$;
5. $B_{\text{cut1}}^{(h,m)}=B_{\text{cut2}}^{(h,m)}=B_{\text{cut3}}^{(h,m)}\leftarrow 10^6$;
6.   **while** $B_{\text{cut1}}^{(h,m)}+B_{\text{cut2}}^{(h,m)}+B_{\text{cut3}}^{(h,m)}\neq 0$ **do**
7. $h \leftarrow h+1$;
8.   Optimize {M-1, M-2} to obtain $\{f_{\text{1,M-1}}^{(h,m)}, f_{\text{2,M-1}}^{(h,m)}\}$ and $\{\boldsymbol{x}^{(h,m)}, \boldsymbol{y}^{(h,m)}, \boldsymbol{z}^{(h,m)}, \boldsymbol{\varphi}^{(h,m)}\}$;
9.   Simulate $\psi_{\text{MMTAM}}(\cdot)$ in M-S1 based on $\boldsymbol{x}^{(h,m)}$, to obtain $\{\boldsymbol{P}_{\text{M-S1}}^{\text{FCS},\tau(h,m)}, \boldsymbol{P}_{\text{M-S1}}^{\text{CP},\tau(h,m)}, f_{\text{1,M-S1}}^{(h,m)}, f_{\text{2,M-S1}}^{(h,m)}\}$, and update $B_{\text{cut1}}^{(h,m)}$ with (37);
10.   Optimize M-S2 based on $\{\boldsymbol{y}^{(h,m)}, \boldsymbol{z}^{(h,m)}, \boldsymbol{\varphi}^{(h,m)}\}$ and $\{\boldsymbol{P}_{\text{M-S1}}^{\text{FCS},\tau(h,m)}, \boldsymbol{P}_{\text{M-S1}}^{\text{CP},\tau(h,m)}\}$;
11.   **if** *M-S2 is feasible* **do**
12.   Obtain $f_{\text{S2}}^{(h,m)}$ and update $B_{\text{cut2}}^{(h,m)}$ with (38);
13.   **else**
14.   Optimize M-V to obtain $f_{\text{V}}^{(h,m)}$ and update $B_{\text{cut3}}^{(h,m)}$ with (39);
15.   **end if**
16.   **end while**
17. **end while**

Output: $\{\boldsymbol{x}^{(h,m)}, \boldsymbol{y}^{(h,m)}, \boldsymbol{z}^{(h,m)}, \boldsymbol{\varphi}^{(h,m)}, \boldsymbol{P}_{\text{M-S1}}^{\text{FCS},\tau(h,m)}, \boldsymbol{P}_{\text{M-S1}}^{\text{CP},\tau(h,m)}\}$

V. Case Studies

A. Test Case Description

A test integrated FCSs and PDSs as illustrated in Fig. 4 is employed to validate the effectiveness of the proposed models. In this test case, the traffic network is simplified from an actual district in Guangzhou, China, which covers 94 nodes and 147 arterial roads. The coupling PDS is a 54-bus system [29] with four 110 kV substations (two existing substations with reinforcement possibility and two candidate ones) and 61 feeders (17 existing feeders and 44 candidate feeders). Note that the studied PDS has no renewable energy sources and its power sources can only be updated by reinforcing or installing 110 kV substations.

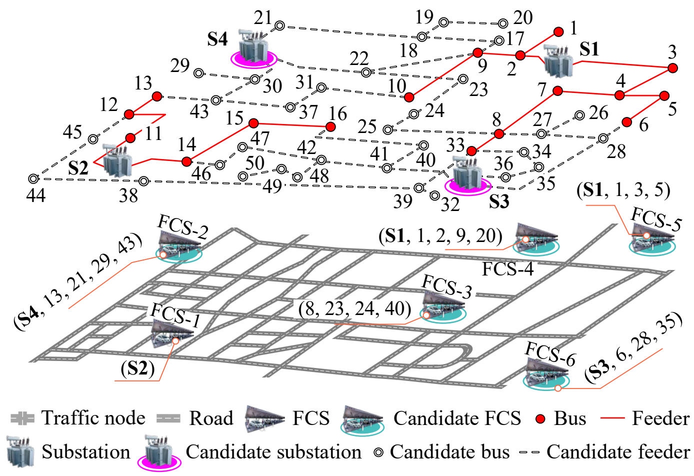

Fig. 4. Initial test integrated FCSs and PDSs. Candidate buses connecting each FCS are listed in the bracket, respectively.

In Fig. 4, the solid (dotted) points and lines denote the existing (candidate) buses/nodes and feeders/roads, respectively. Currently, there is one FCS (FCS-1) connected to the PDS at bus S2. There are five candidate FCSs for future installation, namely FCS-2 to FCS-6, whose connecting buses must be selected from the sets {S4, 13, 21, 29, 43}, {8, 23, 24, 40}, {S1, 1, 2, 9, 20}, {S1, 1, 3, 5}, and {S3, 6, 28, 35}, respectively. The expansion planning of the test integrated system will be divided into three stages with each planning stage lasting three years. The maximum traditional power load is initialized to 49.89 MW and its average growth rate in each stage is 10%. The studied area is assumed to contain 8500 households with a vehicle ownership rate of 1.88 per household, as per the U.S. 2017 national household travel survey [32]. That is, the studied system has 15980 vehicles and 3196 of them are EVs (η^{AG}=20%). The permeability of EVs/agents (η^{AG}) increases by 35% per stage. The reinforcement and installation costs of substations and FCSs are available in [9]. Other specified parameters are shown in Table III.

TABLE III
PARAMETERS LIST

η^{AG} [%]	20	γ [%]	10	σ [\$/(kW·h)]	0.064
$\underline{V}$ [p.u.]	0.95	ω [-]	10^{-6}	$\bar{t}_k$ [min]	35
$\overline{V}$ [p.u.]	1.05	α [%]	30	$\mu^{\text{F},\tau}$ [\$10^4]	16.5
$\underline{n}^{\text{FCS},\tau}$ [-]	1	d^{A} [day]	228	$\mu^{\text{B},\tau}$ [\$10^4/MWA]	3.28

The numerical results and computational time are obtained on a laptop computer with an AMD 1.90-GHz processor and 8 GB of RAM. All simulations and optimizations in this study are

This article has been accepted for publication in a future issue of this journal, but has not been fully edited. Content may change prior to final publication. Citation information: DOI 10.1109/TII.2020.2995742, IEEE Transactions on Industrial Informatics

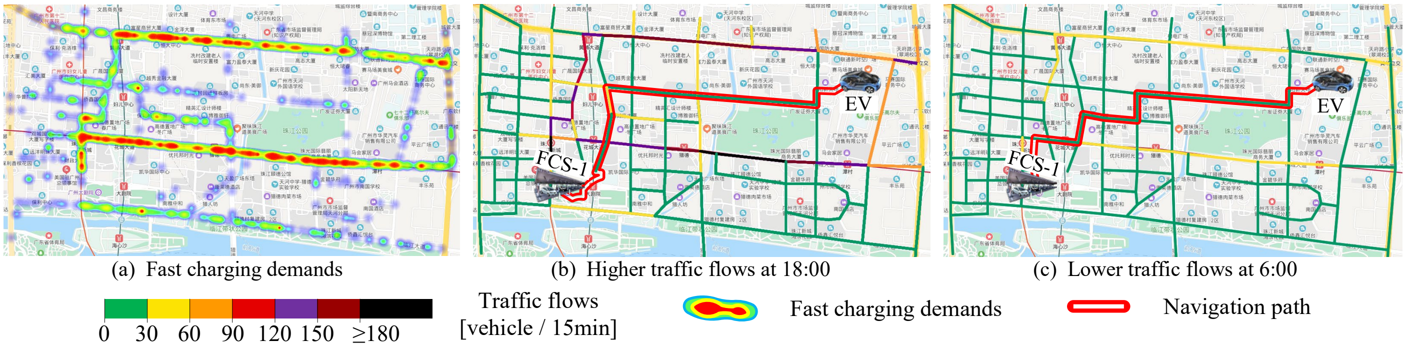

(a) Fast charging demands (b) Higher traffic flows at 18:00 (c) Lower traffic flows at 6:00

Fig. 5. Fast charging demands and traffic flows.

processed though the MATLAB-2014b platform [28] and its built-in YALMIP/CPLEX optimizer [31].

B. Effectiveness of the MMTAM

The simulation proceeds from 0:00 to 24:00 with a 15-min time interval and the average computation time for the MMTAM function $\psi_{\text{MMTAM}}(\bullet)$ is 2.75 s.

Fig. 5 (a) is the Google heat map that marks the locations where EVs send the signal for fast charging demand. Compared with the traffic flows assignments in Fig. 5 (b) and (c), it is concluded that more EVs driving along a road will incur more charging demands. This feature coincides with the statistics that have been applied in [7]-[9] as the basis of siting and sizing new FCSs, i.e., FCSs are more inclined to be installed at crowded roads. Besides, as shown in Fig. 5 (b) and (c), the optimal navigation path to FCSs varies with different levels of traffic flow, which highlights the features of EVs/agents in the proposed MMTAM, i.e., positively respond to real-time surrounding information.

The daily charging loads of private cars and taxis are respectively presented in Fig. 6 (a) and (b). The simulated fast and slow charging loads both obey multivariate normal distributions, which are consistent with the typical features of EV loads [22], [25]. Besides, the real charging loads in this district are further compared in Fig. 6. The comparison clearly shows that the simulated loads are similar to the real data. Hence, the proposed MMTAM is feasible and effective to simulate the driving/charging behaviors of different types of EVs.

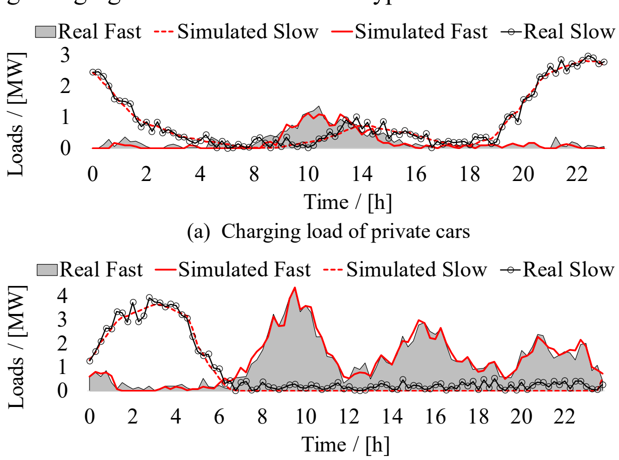

(a) Charging load of private cars

(b) Charging load of taxis

Fig. 6. Simulated daily charging loads of different types of EVs.

Furthermore, on top of the same traffic network and parameters, a comparison is made among the real data, well-established user-equilibrium model [11], and the proposed MMTAM. The daily traffic flows and average speeds are compared in Fig. 7 (a) and (b), respectively. The comparison clearly confirms that the proposed MMTAM is an effective method in terms of traffic flow assignment modeling.

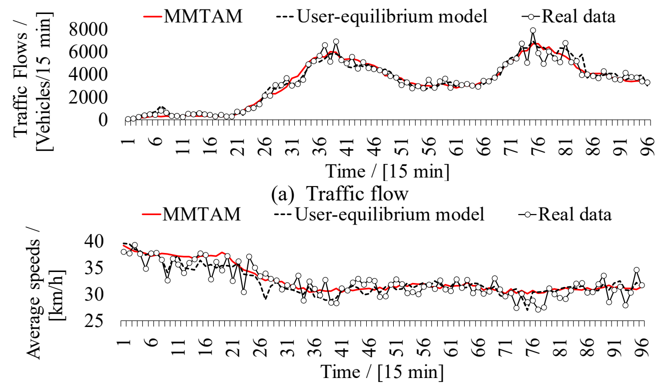

(a) Traffic flow

(b) Average speed

Fig. 7. Comparison among the real data, user-equilibrium model, and the proposed MMTAM.

A numerical comparison based on the gray correlation coefficient [33] is employed to analyze the results shown in Fig. 6 and Fig. 7. The gray correlation coefficients of different curves are respectively listed in Table IV. It is demonstrated in Table IV that the proposed MMTAM performs well in simulating traffic flows and EV charging loads because of its high similarity with the actual data and well-established benchmark approaches.

In summary, benefit from the mechanism that charging loads (calculated by $\lambda_{k,t}$, Equations (8)-(9)) and traffic flows (calculated by $\xi_{k,ij,t-1}$, Equation (9)) both vary with agents' driving paths, the proposed MMTAM successfully reveals the inherent connection between charging loads/FCS operations and traffic flows. This feature highlights the contribution of MMTAM when compared to existing methods of the EV load simulation [22], [25] and traffic flow assignment [9], [13], [14].

TABLE IV
THE SIMILARITY OF SIMULATED RESULT BETWEEN MMTAM AND EXISTING APPROACHES

Curves	Existing approaches	Gray correlation coefficient
EV charging loads	Real data	0.8718 (Fast); 0.8934 (Slow)
	Monte Carlo [22]	0.8671 (Fast); 0.8855 (Slow)
	Trip-chain [23]	0.8544 (Fast); 0.8702 (Slow)
Daily Traffic flows	Real data	0.8878
	User-equilibrium [9]	0.9114
Average speed	Real data	0.8581
	User-equilibrium [9]	0.8865

* All existing approaches are compared with the proposed MMTAM.

C. Joint Planning Results

In the joint planning model, the time interval Δt is set to 1 h. A set of Pareto optimal planning solutions can be obtained by

This article has been accepted for publication in a future issue of this journal, but has not been fully edited. Content may change prior to final publication. Citation information: DOI 10.1109/TII.2020.2995742, IEEE Transactions on Industrial Informatics

altering the learning factor θ. The Pareto frontier is demonstrated in Fig. 8. In a realistic project, the final installation plan will be selected from the Pareto frontier with the planner's special considerations. Without loss of generality, the solution of θ=0.5 is selected as the final plan of the sample integrated FCSs and PDSs and further discussed as follows.

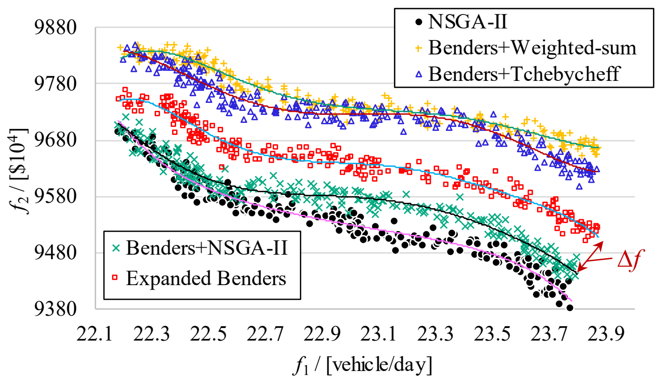

Fig. 8. Pareto frontiers of the joint planning obtained by five different algorithms. The unit "vehicle/day" denotes the average daily deviation between the traffic flow and the equilibrium value αc_{ij} for each road.

The extended topology of the sample integrated system is presented in Fig. 9, and the statistics of the selected planning results are given in Table V. In Table V, new substations S3 and S4 will be respectively installed at stages 2 and 1 to supply the increasing power demand. Besides, all substations {S1, S2, S3, S4} also require extra reinforcement capacities throughout the planning stages. All of these installations are accounted for as f^{C} of Table V. Meanwhile, growing power demands and enlarging network also tend to increase the power loss cost f^{Δ} stage by stage. In terms of FCSs planning, the numbers of installed fast charging devices, i.e., N_q^{τ}, at each stage are 9, 12, and 17, respectively. Note that FCS-4 has not been installed due to the trade-off between cost and traffic unbalance.

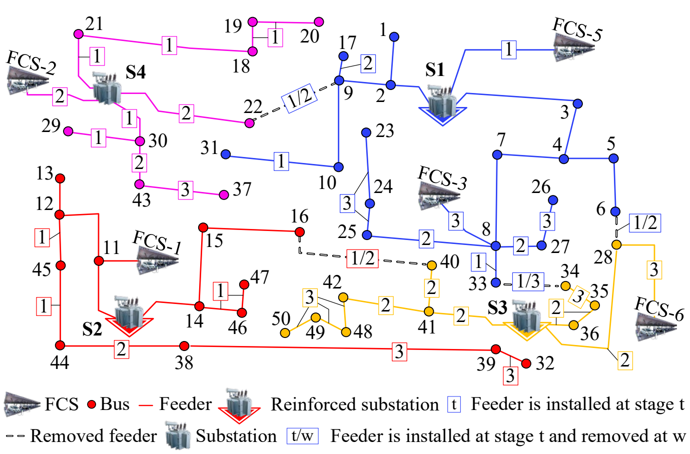

Fig. 9. The extended topology of the sample integrated FCSs and PDSs.

Note that the installation of FCSs fails to halt the increase of f^{UB} in Table V. This is due to the installed number of FCSs that can not match the increasing speed of EVs (35% per stage). In fact, if the unbalance of traffic flow assignment (i.e., $\Re(\cdot)$ in Section III.A) is not considered, the traffic unbalances will become much worse, as will be discussed in Section V.E.

Finally, Fig. 10 shows the daily voltage profiles of the extended PDSs at each planning stage.

In Fig. 10, the selected plan can cover increasing loads and keep voltages staying within the operating limits. This is because the sub-models for PDSs planning, i.e., M-S2 and M-V, are solved by the CPLEX solver, whose built-in optimization algorithm can ensure voltage magnitude constraints to be strictly followed as long as the optimal solution is found [34].

TABLE V
DETAILED PLANNING RESULTS FOR EACH STAGE

Results		Stages 1	2	3
N_q^{τ} / connected bus of FCSs		9/S1 (FCS-5)	12/S4 (FCS-2)	6/8 (FCS-3); 11/28 (FCS-6)
f^{UB} [vehicle/day]		6.8472	7.3848	8.7048
f^{FCS} [10^4]		266.34	125.51	379.04
f^{C} [10^4]		2785.70	2347.35	2113.96
f^{Δ} [10^4]		394.54	566.02	654.75
Substation installation [MVA]	S3	--	12.50	--
	S4	12.50	--	--
Substation reinforcement [MVA]	S1	3.15	4.00	6.30
	S2	3.15	3.15	6.30
	S3	--	--	4.00
	S4	--	3.15	0

* The names of selected candidate FCSs at each stage are noted in brackets.

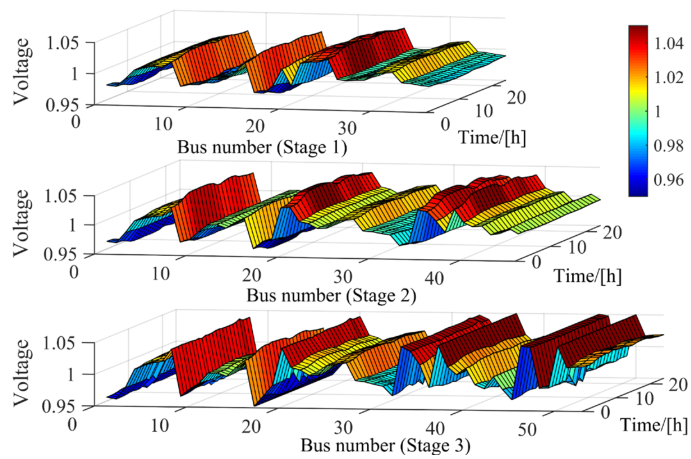

Fig. 10. Voltage profiles of the extended PDSs at each planning stage.

D. Performance of the Bilayer Expanded Benders Algorithm

For the studied integrated system case in Fig. 4, the proposed bilayer expanded Benders algorithm takes four rounds in the outer-layer to obtain the converged results, as displayed in Fig. 11. The convergence properties in Fig. 11 verify the effectiveness of introducing new constraints (32) and (34) to handle the error between two objectives (f_1 and f_2).

Meanwhile, multiple inner-layer iterations are needed in each round of outer-layer optimizations to obtain the optimal planning results for all three planning stages. For instance, during the final round of outer-layer optimizations, i.e., m=4, the detailed convergence process is shown in Fig. 12. In Fig. 12, the gap between the upper and lower bounds remains constant for the first few iterations, because the slave model M-S2 is infeasible and model M-V must be solved to generate feasibility cuts. As the iterations continue, M-S2 eventually becomes feasible and the gap begins to decrease until the convergence criterion, i.e., (40), is met.

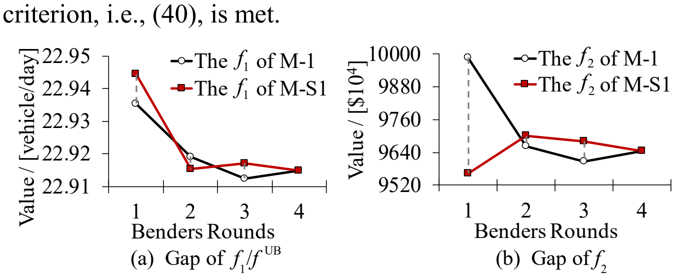

Fig. 11. Evolution of gaps between M-1 and M-S1.

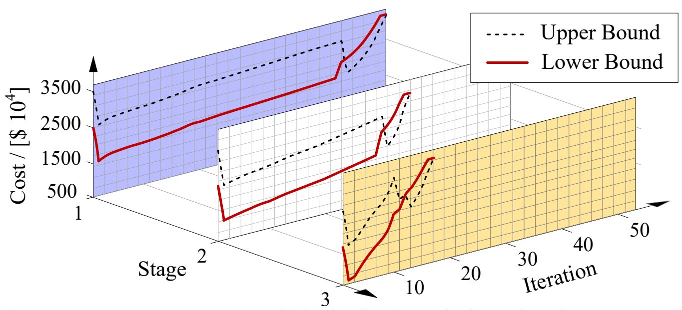

Fig. 12. Convergence process within the final round of Benders decomposition.

To highlight the advantages of our algorithm, four commonly used algorithms, i.e., the NSGA-II, "Benders+Weighted-sum", "Benders+Tchebycheff", and "Benders+NSGA-II", are respectively compared. Among them, the traditional Benders decomposition must combine with another algorithm to solve M-0 because it cannot handle multiple objectives. The evolution performances are compared in the following two aspects:

- *Optimality*. The Pareto front of NSGA-II in Fig. 8 is selected as the benchmark. The relative Euclidean distance between the optimized Pareto front and the benchmark serves as a new index (Δf) to evaluate the optimality. Δf can be calculated as:

$$\Delta f = \sqrt{\left(f_1/f_1^{\text{NSGA-II}} - 1\right)^2 + \left(f_2/f_2^{\text{NSGA-II}} - 1\right)^2}$$

- *Robustness*. Each multi-objective optimization algorithm will be executed 10 times, thus obtaining 10 Pareto fronts. By replacing $f_1^{\text{NSGA-II}}$ in the formula Δf with the average Pareto front, the robustness index of each algorithm can be obtained. A larger (smaller) robustness index indicates the algorithm is less (more) robust.

As shown in Table VI, the proposed algorithm offers higher better optimality compared to "Benders+Weighted-sum" and "Benders+Tchebycheff" methods. Compared to the NSGA-II based methods which have the best optimality, the proposed algorithm has a significant advantage in terms of improving computational efficiency. From the algorithm robustness perspective, the proposed bilayer Bender decomposition is the most robust algorithm. The poor robustness of NSGA-II based algorithms lies in their random evolution process.

TABLE VI
DETAILED COMPARISON AMONG FOUR DIFFERENT ALGORITHMS

Algorithm	Benders iteration	Average time [h]	Average Δf of Pareto front	Robustness
NSGA-II	N/A	8.41	0%	0.195%
Benders+Weighted-sum	125	0.72	0.8848%	0.076%
Benders+Tchebycheff	143	1.58	0.8615%	0.085%
Benders+NSGA-II	192	7.35	0.2313%	0.143%
Bilayer expanded Benders	413	3.74	0.4401%	0.072%

In summary, the proposed algorithm demonstrates the highest robustness and can efficiently provide a Pareto front with satisfactory optimality.

E. Comparative Study

A software package has been developed based on JavaScript and Python to perform the proposed joint planning task on real-world systems. The computation is performed in the MATLAB platform, while the data input/output is done through a web-based interface. This software package has been employed by utility companies such as the China Southern Power Grid in PDS and FCS planning. Due to space limitation, more details about the software implementation can be provided upon request.

To validate the effectiveness of the proposed model in other cases, a practical large-scale integrated FCSs and PDSs in Wenzhou, China, is simulated as a comparative study. The heat map of charging demands is demonstrated in Fig. 13 as an output of the developed software.

The following four test cases are studies to demonstrate the effectiveness of a joint planning strategy and the introduced MMTAM method.

Case 1: The PDS and FCSs are independently planned based on the sub-models proposed in Sections III.B and C.

Case 2: The joint planning strategy proposed in this paper.

Case 3: The joint planning strategy based on a user-equilibrium traffic flow model described in [9].

Case 4: The joint planning strategy with random slow charging, i.e., expectation variables $\beta_{u,k,t}$ in (9) are all set to "1".

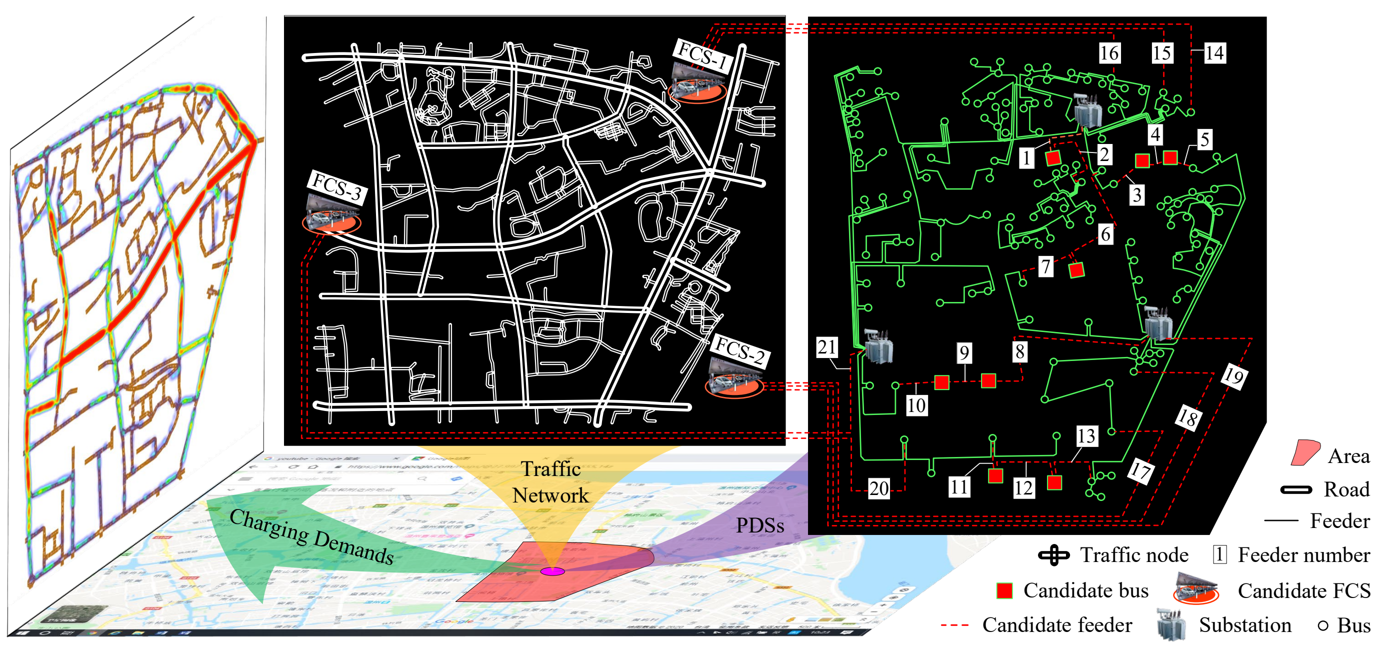

Fig. 13. A realistic large-scale sample integrated FCSs and PDSs in Wenzhou, China.

This article has been accepted for publication in a future issue of this journal, but has not been fully edited. Content may change prior to final publication. Citation information: DOI 10.1109/TII.2020.2995742, IEEE Transactions on Industrial Informatics

All four cases are simulated for one planning stage of one year, and the results are compared in Table VII. Several observations can be made from Table VII and are discussed below:

- f^{UB} in cases {1, 2, 4} are significantly lower than in case 3, which indicates the proposed MMTAM can efficiently balance the traffic flow assignment. To obtain the lowest f^{UB}, case 1 has higher f^{FCS}, f^{C}, and f^{Δ} when planning the investment of PDS and FCSs than cases {2, 4}.
- Due to the absence of MMTAM, case 3 prefers to install FCSs on the crowded roads to capture the most intense traffic flows. As a consequence, case 3 not only has the worst traffic condition but also a higher FCS investment cost than cases {2, 4} (about {83.12, 68.35}×$\$10^4$). Because it is generally expensive to rent a certain square of land in a crowded place to install FCSs.
- The total costs of cases 1-4 are {2.92, 2.67, 2.59, 2.80}×$\$10^7$, respectively. Therefore, the joint planning of cases {2, 3, 4} are considerably more cost-efficient than the independent planning case 1.
- Benefit from the ordered slow charging loads, the PDSs in case 2 keep stable operation even with lower safety capacity, which helps to save more investment costs than case 4 (about $\$128.45\times10^4$).
- Although it is not the most economic, the proposed multi-objective approach in case 2 achieved a good trade-off between balancing traffic flows and saving investment costs, which brings a considerable extra social benefit to traffic networks.

TABLE VII
COMPARISON OF OPTIMAL SOLUTIONS FOR FOUR CASES

Case	Selected feeders	f^{UB} [vehicle/day]	Costs [$\$10^4$] Total	f^{FCS}	f^{C}	f^{Δ}
1	1-3-4-6-8-10-11-12-17-20	11.2477	2921.12	596.52	1916.25	408.35
2	1-3-4-6-9-10-11-13-17-21	12.0682	2671.77	483.05	1808.10	380.62
3	2-4-5-7-8-9-11-13-14-18	16.9315	2587.89	566.17	1653.69	368.03
4	2-3-4-6-9-10-11-13-15-18	11.8767	2800.22	497.82	1904.57	397.83

* Installed candidate bus/FCS is omitted here since it can be obtained through the connecting feeder, as shown in Fig. 13.

Furthermore, to relieve the concern in the impacts of charging load levels on our observations, the cost-benefit is analyzed with the net present value (Φ^{NPV}) [36]. The lifetime of PDSs is set to 10 years. The net present values of cases 1-4 with different permeability (η^{AG}) are compared in Table VIII, respectively.

TABLE VIII
NET-PRESENT VALUES OF CASES 1-4 WITH DIFFERENT PERMEABILITY

Initially η^{AG} [%]	Final η^{AG} [%]	Cases (1-2)/2	Case 2 [$\$10^4$]	Cases (3-2)/2	Cases (4-2)/2
10	18.23	-0.1307	1401.08	0.0812	-0.0807
20	36.45	-0.1943	1283.32	0.0654	-0.1001
30	54.68	-0.2708	1165.60	0.0464	-0.1234
40	72.90	-0.3644	1047.91	0.0231	-0.1519
50	91.13	-0.4818	930.26	-0.0061	-0.1876

* *Cases (1-2)/2* means the relative deviation of cases {1, 2}, which calculated by comparing their net present values (Φ^{NPV}), then divided by Φ^{NPV} of case 2.

The comparisons in Table VIII support the abovementioned observations. Besides, with ever-growing charging loads/η^{AG}, more observations are obtained:

- The necessity of joint planning is highlighted since the relative deviations of cases {1, 2} keeps increasing.
- The advantage of case 3 in cost-saving is gradually overtaken by case 2. Case 2, i.e, the proposed joint planning, becomes the most economical approach when the initial η^{AG}=50%.
- It becomes more important to manage slow charging behaviors when facing a higher initial η^{AG}, as indicated by the increasing deviations between case 2 and case 4.

VI. CONCLUSION

A joint planning strategy considering unbalanced traffic flow is developed in this paper. To properly model the traffic flow assignment, a novel microscopic method namely MMTAM is first proposed to integrate the simulations of EV charging loads and traffic flows. The MMTAM is capable of revealing the influences of FCS investments on traffic flows, which lays the foundation for our multi-objective planning model that balances the interests of PDSs, FCSs, and traffic networks simultaneously. A new bilayer expanded Benders algorithm is then developed to solve the multi-objective planning model. The performance of the proposed model is validated through two real-world test systems in China. The simulation results also conclude that:

- the proposed MMTAM method is effective in modeling the connections between EV charging loads and traffic flows;
- the developed algorithm overcomes the drawback of traditional Benders decompositions in handling multiple objectives, which performs better than other optimization algorithms in terms of improving solving efficiency and robustness;
- the proposed multi-objective joint planning model can achieve an efficient trade-off between relieving traffic congestion and reducing planning cost.

In addition to the charging behaviors, the vehicle-to-grid capability of EVs is believed to a promising solution in terms of smoothing renewable energy fluctuation, providing ancillary services, etc. The impacts of vehicle-to-grid on EV charging behaviors and FCS planning will be explored in our future work.

REFERENCES

[1] M. J. Sanjari, H. B. Gooi, and N. Nair, "Power generation forecast of hybrid PV-wind system," *IEEE Trans. Sustain. Energy*, early access, 2019.

[2] China's Leader in Online Legal Research, "Notice of the state council on issuing the planning for the development of the energy-saving and new energy automobile industry (2012-2020)," 2019 [Online]. Available: http://www.lawinfochina.com/display.aspx?lib=law&id=10732&CGid=.

[3] Gov.uk, "Road to Zero Strategy," 2019 [Online]. Available: https://assets.publishing.service.gov.uk/government/uploads/system/uploads/attachment_data/file/739460/road-to-zero.pdf.

[4] Y. Parvini, A. Vahidi, and S. A. Fayazi. "Heuristic versus optimal charging of supercapacitors, Lithium-ion, and Lead-acid batteries: an efficiency point of view," *IEEE Trans. Contr. Syst. Tech.*, vol. 26, no. 1, pp. 167-180, Jan. 2018.

[5] Y. Zhang, J. Chen, L. Cai, and J. Pan, "Expanding EV charging networks considering transportation pattern and power supply limit," *IEEE Trans. Smart Grid*, vol. 10, no. 6, pp. 6332-6342, Nov. 2019.

[6] H. Zhang, S. J. Moura, Z. Hu, W. Qi, and Y. Song, "A second order cone programming model for planning PEV fast-charging stations," *IEEE Trans. Power Syst.*, vol. 33, no. 3, pp. 2763-2777, May 2018.

[7] H. Zhang, S. J. Moura, Z. Hu, and Y. Song, "PEV fast-charging station siting and sizing on coupled transportation and power networks," *IEEE Trans. Smart Grid*, vol. 9, no. 4, pp. 2595-2605, Jul. 2018.

[8] M. O. Badawy and Y. Sozer, "Power flow management of a grid tied PV-battery system for electric vehicles charging," *IEEE Trans. Indus. Appl.*, vol. 53, no. 2, pp. 1347-1357, Mar.-Apr. 2017.

[9] W. Yao, J. Zhao, F. Wen, Z. Dong, Y. Xue, Y. Xu, and K. Meng, "A multi-objective collaborative planning strategy for integrated power distribution and electric vehicle charging systems," *IEEE Trans. Power Syst.*, vol. 29, no. 4, pp. 1811-1821, Jul. 2014.

This article has been accepted for publication in a future issue of this journal, but has not been fully edited. Content may change prior to final publication. Citation information: DOI 10.1109/TII.2020.2995742, IEEE Transactions on Industrial Informatics

[10] S. Wang, Z. Dong, F. Luo, K. Meng, and Y. Zhang, “Stochastic collaborative planning of electric vehicle charging stations and power distribution system,” *IEEE Trans. Indus. Info.,* vol. 14, no. 1, pp. 321-331, Jan. 2018.

[11] W. Wei, L. Wu, J. Wang, and S. Mei, “Network equilibrium of coupled transportation and power distribution systems,” *IEEE Trans. Smart Grid*, vol. 9, no. 6, pp. 6764-6779, Nov. 2018.

[12] W. Wang, J. Xi, and D. Zhao, “Learning and inferring a driver's braking action in car-following scenarios,” *IEEE Trans. Veh. Tech.*, vol. 67, no. 5, pp. 3887-3899, May 2018.

[13] M. A. I. Tsompanas, G. C. Sirakoulis, and A. I. Adamatzky, “Evolving transport networks with cellular automata models inspired by slime mould,” *IEEE Trans. Cybern.*, vol. 45, no. 9, pp. 1887-1899, Sep. 2015.

[14] Z. Zhou, B. D. Schutter, S. Lin, and Y. Xi, “Two-level hierarchical model-based predictive control for large-scale urban traffic networks,” *IEEE Trans. Contr. Syst. Tech.*, vol. 25, no. 2, pp. 496-508, Mar. 2017.

[15] K. Chaudhari, N. K. Kandasamy, A. Krishnan, A. Ukil, and H. B. Gooi, “Agent-based aggregated behavior modeling for electric vehicle charging load,” *IEEE Trans. Indus. Info.,* vol. 15, no. 2, pp. 856-868, Feb. 2019.

[16] R. Wang, Z. Zhou, H. Ishibuchi, T. Liao, and T. Zhang, “Localized weighted sum method for many-objective optimization,” *IEEE Trans. Evolu. Comp.*, vol. 22, no. 1, pp. 3-18, Feb. 2018.

[17] X. Ma, Q. Zhang, G. Tian, J. Yang, and Z. Zhu, “On Tchebycheff decomposition approaches for multiobjective evolutionary optimization,” *IEEE Trans. Evolu. Comp.*, vol. 22, no. 2, pp. 226-244, Apr. 2018.

[18] Y. Yao, Z. Peng, and B. Xiao, "Parallel hyper-heuristic algorithm for multi-objective route planning in a smart city," *IEEE Trans. Veh. Tech.*, vol. 67, no. 11, pp. 10307-10318, Nov. 2018.

[19] X. Tan, G. Qu, B. Sun, N. Li, and D. H. K. Tsang, “Optimal scheduling of battery charging station serving electric vehicles based on battery swapping,” *IEEE Trans. Smart Grid*, vol. 10, no. 2, pp. 1372-1384, Mar. 2019.

[20] H. Zhang, S. J. Moura, Z. Hu, W. Qi, and Y. Song, “Joint PEV charging network and distributed PV generation planning based on accelerated generalized Benders decomposition,” *IEEE Trans. Transp. Electrif.*, vol. 4, no. 3, pp. 789-803, Sep. 2018.

[21] A. Banerjee, A. Paul, and S. P. Maity, “Joint power allocation and route selection for outage minimization in multihop cognitive radio networks with energy harvesting,” *IEEE Trans. Cogn. Commun. Netw.*, vol. 4, no. 1, pp. 82-92, Mar. 2018.

[22] C. She, Z. Wang, F. Sun, P. Liu, and L. Zhang, “Battery aging assessment for real-world electric buses based on incremental capacity analysis and radial basis function neural network,” *IEEE Trans. Ind. Inform.,* vol. 16, no. 5, pp. 3345-3354, May 2020.

[23] H. Yang, Y. Deng, J. Qiu, M. Li, M. Lai, and Z. Dong, “Electric vehicle route selection and charging navigation strategy based on crowd sensing,” *IEEE Trans. Indus. Info.,* vol. 13, no. 5, pp. 2214-2226, Oct. 2017.

[24] J. Yang, Y. Xu, and Z. Yang, “Regulating the collective charging load of electric taxi fleet via real-time pricing,” *IEEE Trans. Power Syst.*, vol. 32, no. 5, pp. 3694-3703, Sep. 2017.

[25] Q. Liang, L. Lin, B. Zhou, and W. Zhao, “Modeling of PEV charging load based on trip chain theory and the impact of PEV on distribution networks,” in *Proc. International Conf. on Power System Technology (POWERCON)*, Guangzhou, China, Nov. 2018.

[26] C. Luo, Y. Huang, and V. Gupta, “Stochastic dynamic pricing for EV charging stations with renewable integration and energy storage,” *IEEE Trans. Smart Grid*, vol. 9, no. 2, pp. 1494-1505, Mar. 2018.

[27] H. Liu, J. Qi, J. Wang, P. Li, C. Li, and H. Wei, “EV dispatch control for supplementary frequency regulation considering the expectation of EV owners,” *IEEE Trans. Smart Grid*, vol. 9, no. 4, pp. 3763-3772, Jul. 2018.

[28] MathWorks, “Support-Documentation,” [Online]. Available: https://www.mathworks.com/help/matlab/index.html.

[29] V. Miranda, J. V. Ranito, and L. M. Proenca, “Genetic algorithms in optimal multistage distribution network planning,” *IEEE Trans. Power Syst.*, vol. 9, no. 4, pp. 1927-1933, Nov. 1994.

[30] H. G. Yeh, D. F. Gayme, and S. H. Low, “Adaptive VAR control for distribution circuits with photovoltaic generators,” *IEEE Trans. Power Syst.*, vol. 27, no. 3, pp. 1656-1663, Aug. 2012.

[31] YALMIP, “Tutorials,” [Online]. Available: https://yalmip.github.io/tutorials/.

[32] N. M. Guckin and A. Fucci, “Summary of Travel Trends: 2017 National Household Travel Survey,” U.S. Department of Transportation Federal Highway Administration, Washington, DC, USA, Tech. Rep. FHWA-PL-18-019, Jul. 2018.

[33] A. Acır, M. E. Canlı, İ. Ata, and R. Çakıroğlu, “Parametric optimization of energy and exergy analyses of a novel solar air heater with grey relational analysis,” *Appl. Therm. Eng.*, vol. 122, pp. 330-338, Jul. 2017.

[34] K. Deb, L. Zhu, and S. Kulkarni, “Handling multiple scenarios in evolutionary multiobjective numerical optimization,” *IEEE Trans. Evol. Comp.*, vol. 22, no. 6, pp. 920-933, Dec. 2018.

[35] G. T. Heydt, “The probabilistic evaluation of Net Present value of electric power distribution systems based on the Kaldor–Hicks compensation principle,” *IEEE Trans. Power Syst.*, vol. 33, no. 4, pp. 4488-4495, Jul. 2018.

BIOGRAPHIES

Wentao Yang (S’19) received the B.E. degree in electrical engineering from *Wuhan University*, Wuhan, China, in 2015.

He is currently pursuing the Ph.D. degree in *Zhejiang University*, Hangzhou, China. His main research interests lie in electrical vehicles, integrated multi-energy systems, and Peer-to-Peer energy transactions.

Weijia Liu (M’20) received the B.Eng. and Ph.D. degrees in electrical engineering from *Zhejiang University*, China, in 2011 and 2016, respectively.

He is currently a Researcher with National Renewable Energy Laboratory (NREL) in Golden, Colorado, USA. His research interests include power system restoration and resilience, smart grid, and integrated energy systems.

C. Y. Chung (M’01-SM’07-F’16) received the B.Eng. (with First Class Honors) and Ph.D. degrees in electrical engineering from The Hong Kong Polytechnic University, Hong Kong, China, in 1995 and 1999, respectively.

He is currently a Professor, the NSERC/SaskPower (Senior) Industrial Research Chair in Smart Grid Technologies, and the SaskPower Chair in Power Systems Engineering in the Department of Electrical and Computer Engineering at the University of Saskatchewan, Saskatoon, SK, Canada.

Dr. Chung is currently the Senior Editor of “IEEE Transactions on Power Systems”, Vice Editor-in-Chief of “Journal of Modern Power Systems and Clean Energy”, Subject Editor of “IET Generation, Transmission & Distribution”, Editor of “IEEE Transactions on Sustainable Energy” and “IEEE Power Engineering Letters”, and Editorial Board Member of “CSEE Journal of Power and Energy Systems” and “Protection and Control of Modern Power Systems”. He is also an IEEE PES Distinguished Lecturer and a member of IEEE PES Fellows Evaluation Committee.

Fushuan Wen (SM’07) received the B.E. and M.E. degrees from *Tianjin University*, Tianjin, China, in 1985 and 1988, respectively, and the Ph.D. degree from *Zhejiang University*, Hangzhou, China, in 1991, all in electrical engineering.

He joined the faculty of *Zhejiang University* in 1991, and has been a full professor since 1997. He is also a part-time distinguished professor under Yusheng XUE Education Foundation in *Hangzhou Dianzi University*, Hangzhou, China. He had been a university distinguished professor, the deputy dean of the School of Electrical Engineering and the director of the Institute of Power Economics and Electricity Markets in *South China University of Technology*, Guangzhou, China, from 2005 to 2009. He is a professor in the Department of Electrical Power Engineering and Mechatronics, *Tallinn University of Technology*, taking leave from Zhejiang University. His research interests lie in power industry restructuring, power system alarm processing, fault diagnosis and restoration strategies, as well as smart grids and electric vehicles.

Prof. Wen is the Editor-in-Chief of *IET Energy Conversion and Economics*, and a deputy Editor-in-Chief of *Automation of Electric Power Systems*. He also serves as the editor, subject editor and associate editor of a few international journals.